Computer Modeling in Engineering & Sciences

Tech Science Press

Doi:10.32604/cmes.2025.065442

ARTICLE

Pareto Multi-Objective Reconfiguration of IEEE 123-Bus Unbalanced Power Distribution Networks Using Metaheuristic Algorithms: A Comprehensive Analysis of Power Quality Improvement

Nisa Nacar Çıkan*

Electrical and Electronics Engineering Department, Cukurova University, Adana, 01250, Türkiye

*Corresponding Author: Nisa Nacar Çıkan. Email: ncikan@cu.edu.tr

Received: 13 March 2025; Accepted: 27 May 2025; Published: 30 June 2025

ABSTRACT: This study addresses the critical challenge of reconfiguration in unbalanced power distribution networks (UPDNs), focusing on the complex 123-Bus test system. Three scenarios are investigated: (1) simultaneous power loss reduction and voltage profile improvement, (2) minimization of voltage and current unbalance indices under various operational cases, and (3) multi-objective optimization using Pareto front analysis to concurrently optimize voltage unbalance index, active power loss, and current unbalance index. Unlike previous research that oftensimplified system components, this work maintains all equipment, including capacitor banks, transformers, and voltage regulators, to ensure realistic results. The study evaluates twelve metaheuristic algorithms to solve the reconfiguration problem (RecPrb) in UPDNs. A comprehensive statistical analysis is conducted to identify the most efficient algorithm for solving the RecPrb in the 123-Bus UPDN, employing multiple performance metrics and comparative techniques. The Artificial Hummingbird Algorithm emerges as the top-performing algorithm and is subsequently applied to address a multi-objective optimization challenge in the 123-Bus UPDN. This research contributes valuable insights for network operators and researchers in selecting suitable algorithms for specific reconfiguration scenarios, advancing the field of UPDN optimization and management.

KEYWORDS: Voltage and current unbalanced index; unbalanced power distribution network; power quality; metaheuristic algorithms; reconfiguration; optimization

1 Introduction

Network reconfiguration is a crucial technique in the operation and planning of power distribution networks (PDNs), aiming to enhance efficiency and reliability while minimizing power losses. As the final link between power utilities and consumers, distribution systems must adapt to increasing load demands, which complicate operations and increase losses. Reconfiguration alters the topological configuration of the network by changing the operational statuses of sectionalizing switches (SSs) and tie switches (TSs), thereby balancing loads and enhancing performance [1]. This method is cost-effective and requires minimal additional equipment compared to other strategies such as capacitor placement or distributed generation (DG) allocation [2]. It maintains the network's radial topology, essential for protection and maintenance, while optimizing the system for loss minimization and load balancing [3].

In power distribution systems, the reconfiguration problem (RecPrb) is typically solved using four key techniques. These methods are modern, heuristic, classical (deterministic), and metaheuristic [4]. Modern techniques employ cutting-edge tools such as artificial intelligence (AI), the Internet of Things (IoT), and

machine learning to generate creative and dynamic solutions. Heuristic techniques generate faster solutions by working with the problem's basic characteristics. Deterministic approaches depend on mathematical formulations that need continuously differentiable objective functions with gradient data to direct the optimization. Although classical methods provide efficient convergence and accurate solutions for tractable problems, they often fail when confronted with real-world scenarios involving discontinuous or highly non-linear functions. Metaheuristic techniques are inspired by natural processes and use probability-based strategies to navigate solution spaces. All four approaches provide valuable benefits for solving RecPrb. Metaheuristic algorithms have become one of the most widely studied methods recently. Their popularity comes from being nature-inspired problem-solvers that efficiently explore complex systems. This makes them highly effective for key objectives like minimizing power loss and enhancing voltage stability [5]. Metaheuristic algorithms can mainly be divided into two groups: single-solution-based and population-based [6]. Population-based algorithms use a group of solutions to find the best result. These algorithms can be grouped into five main categories based on their inspiration. The first group is swarm intelligence-based, which is inspired by the collective behavior of animals like birds, fish, or insects. The second group is evolution-based, which follows processes like mutation and selection, similar to natural evolution. The third one is physics-based, where algorithms use ideas from physical laws, such as gravity or motion. The fourth group is human behavior-based, which copies how people act in social, political, or learning situations. Finally, there is a fifth group called biological or ecological nature-based, which includes algorithms inspired by living organisms that don't fit the other groups. For example, the Fungal Growth Optimizer (FGO) is inspired by how fungi grow in nature, so it belongs to this fifth group [6]. The Artificial Satellite Search Algorithm (ASSA) follows the motion of satellites and is based on physics, so it fits in the physics-based category [7].

The RecPrb has been extensively studied in the literature, with numerous optimization techniques proposed to address this challenge. Comprehensive reviews of previous research on RecPrbs have been provided in [8,9]. However, despite the long-standing interest in PDN reconfiguration, a careful examination of the existing literature reveals that most studies consider distribution networks as balanced power distribution systems. In this approach, the balanced modeling typically simplifies the unbalanced system into either a positive sequence system or separates it into three individual single-phase networks [10]. While this balanced approach has been widely used due to its simplicity, it may not accurately represent the complexities of real-world distribution networks, which are often inherently unbalanced. Recent studies on balanced power distribution network reconfiguration problems show significant advancements in optimization techniques and problem formulation.

For instance, a thorough comparative study was conducted in [11] statistically assessing the effectiveness of 11 widely used metaheuristic algorithms with respect to system reliability enhancement and power loss minimization. These algorithms were evaluated on four distinct balanced test systems. Several other notable studies have contributed to the field using balanced test systems. In [12], a hybrid approach combining plant growth simulation algorithm and particle swarm optimization was proposed for power loss minimization in radial distribution networks. The method was tested on IEEE 33-bus and 69-bus systems, demonstrating superior results with the integration of multiple DGs along with network reconfiguration. In [13], a novel multi-objective bidirectional co-evolutionary algorithm was introduced for dynamic multi-objective network reconfiguration with DG allocation. The approach was applied to 33-bus and 118-bus radial test systems, achieving significant improvements in voltage profile and power loss reduction. In [14], an iterative bi-level scheduling approach for stochastic distribution networks was developed, combining multi-step reconfiguration with many-objective reduction. The method was tested on 33-node, 84-node, 119-node, and 136-node systems, demonstrating notable reductions in network loss and voltage deviation. Despite these

advancements in balanced PDN reconfiguration, there is growing recognition of the need to address the challenges posed by unbalanced systems, which more accurately reflect real-world conditions.

The study of unbalanced three-phase PDN reconfiguration is crucial for addressing real-world power distribution challenges, as most practical systems exhibit some degree of imbalance. Most research on unbalanced three-phase PDN reconfiguration has concentrated on smaller-scale test systems, including 25-bus and 19-bus systems. For instance, reference [15] introduced a method for reconfiguring unbalanced 69-bus and 33-bus test systems aimed at reducing energy not supplied index (ENS), voltage unbalance index (VUI), and power loss using an Improved Coronavirus Herd Immunity Optimizer algorithm. In [16], a 24-h reconfiguration model for a 34-bus test system was presented using mixed-integer linear programming. Reference [17] introduced a Firefly algorithm utilizing a fuzzy domain approach to reduce bus voltage deviation and losses in 25-bus and 19-bus unbalanced power distribution network (UPDN). Reference [18] employed reinforcement learning to formulate the RecPrb for 13-bus and 34-bus test systems.

Research on more complex networks, including the 123-Bus test system, is less common because of their significant complexity and analytical challenges. The 123-Bus test system represents a more practical and challenging scenario for UPDN reconfiguration. Some notable works on the 123-Bus UPDN include: applied a robust deep learning-based approach that focuses on uncertainties in PDN [3], which developed a reconfiguration technique under post-fault and normal conditions [19], which presented an enhanced power flow technique based on backward-forward (BF) sweep method [20], which performed dynamic reconfiguration employing a selective bat algorithm (SBAT) [21], which proposed a dynamic reconfiguration technique integrated with DG unit uncertainty [22], which considered reliability and power loss in reconfiguration; and which introduced a teaching learning-based optimization (TLBO) technique for simultaneous minimization of net reactive power flow and, real power loss while enhancing voltage stability index and minimizing aggregated voltage deviation index [24]. It is important to note that in several studies [3,19,21–24], the 123-Bus three phase UPDN was modified by eliminating components such as capacitor banks, transformers, and voltage regulators. While this simplification facilitated computational analysis, it may lead to results that do not sufficiently represent the intricate nature of real-world distribution networks. This limitation underscores the need for more comprehensive approaches that maintain the integrity of the original system configuration.

These complexities are particularly evident when considering the challenges posed by unbalanced loads and their impact on power quality in distribution networks. Unbalanced load distribution in PDNs is a significant concern that results in capacity limit violations, elevated energy losses, and deterioration in power quality [17]. Power quality (PQ) encompasses a range of electrical parameters that ensure the reliable and efficient operation of power systems. Key power quality disturbances (PQDs) include voltage sags, swells, interruptions, flicker, harmonics, and voltage and current unbalance [25,26]. Among these, voltage and current unbalance are particularly critical in unbalanced distribution networks, as they can lead to increased energy losses, equipment overheating, reduced operational lifespan, and malfunctioning of protection systems [26]. Several recent studies, including the Improved Transient Search Optimization Algorithm (ITSOA), have addressed these PQ issues directly through network reconfiguration [27] without relying on external devices such as DG or unified power quality conditioner (UPQC), further validating the practical importance of minimizing voltage and current unbalance. As highlighted in recent systematic reviews [25], monitoring and improving these unbalance indices are essential for enhancing power quality in smart grids. Addressing voltage and current unbalance without relying on additional compensation devices, such as UPQC or DG units, offers a practical and cost-effective strategy, especially in large and complex systems like the 123-Bus unbalanced distribution network. This work follows such an approach, aiming to

improve system power quality through topological reconfiguration focused on minimizing the VUI and current unbalance index (CUI).

Current and voltage unbalance (CVU) are serious power quality problems mainly affecting distribution systems [28], and they can pose substantial threats to PDNs and connected equipment [29]. The primary causes of CVU include inherent system attributes, including the uneven allocation of two-phase and single-phase loads across three-phase lines, as well as equipment-related disruptions [28,29]. High levels of CVU can lead to equipment malfunctions, protection device failures, overheating, and reduced operational efficiency [29]. To address these issues and quantify the unbalance in PDNs, there are established standardized metrics: the VUI for measuring voltage imbalance [30], and the CUI for assessing current imbalance. While VUI limits are well-defined in various standards, CUI limits remain less clear [28]. Previous research has explored methods to minimize VUI, such as DG allocation. However, the impact of CUI on system power quality has received less attention, despite its significant effect on electrical machines commonly used in DG implementation [29]. While these standardized metrics provide a foundation for measuring unbalance, recent studies have begun to address both VUI and CUI simultaneously, advancing the field beyond the previous focus on VUI alone. For instance, research in [29] used the iterated local search algorithm to optimize capacitor sizes while limiting both VUI and CUI. Another study [31] examined CUI and VUI metrics at feeder buses following the allocation of DG. However, research on solving the RecPrb in UPDNs while considering VUI and CUI effects remains limited. One notable study [32] addressed the RecPrb in PDNs taking into account the direct effects of CUI and VUI on 25 and 19-bus test systems. The authors also examined a modified 123-Bus test system, albeit with simplified conditions that may not fully reflect real-world scenarios. The most comprehensive study to date on this subject was conducted in [33]. This research utilized the 123-Bus test system without modifications commonly applied in literature, thereby yielding results that more accurately reflect real-world conditions. The study in [33] addressed the challenges posed by unbalanced loads by employing the slime mould algorithm (SMA) [34] for addressing the RecPrb in PDNs. The primary objectives of the study were the reduction of power loss, CUI, and VUI. To assess the efficacy of the SMA method, it was compared to the established Equilibrium Optimizer (EO) [35] and Differential Evolution (DE) [36] algorithms in solving RecPrbs of UPDN.

The reconfiguration of UPDNs presents a complex optimization challenge. As system complexity increases with the number of buses and tie switches, algorithms often struggle to reach the global optimum, becoming trapped in local optima. This escalating complexity underscores the importance of identifying appropriate metaheuristic algorithms capable of overcoming these challenges. The No Free Lunch (NFL) theorem posits that no single algorithm can consistently outperform all others across every problem domain. This principle highlights the critical need to determine the most effective algorithm for each specific problem, particularly in the context of UPDN reconfiguration. In light of this, this study aims to comprehensively evaluate the efficacy of various metaheuristic algorithms in addressing the UPDN reconfiguration problem. Twelve metaheuristic algorithms were selected for analysis in this study. Three of them—DE [36], EO [35], and SMA [34]—have already been used in similar optimization problems and provide a strong baseline for comparison. The remaining nine algorithms are more recent and reflect current developments in the field of optimization. These algorithms were carefully chosen to represent different categories of population-based metaheuristics. For example, the Artificial Hummingbird Algorithm (AHA) [37] is inspired by the foraging behavior of hummingbirds and falls under the swarm intelligence-based category. The Arithmetic Optimization Algorithm (AOA) is a physics-inspired algorithm based on simple mathematical operations. It is tested on 33-bus and 69-bus PDNs with network reconfiguration [38]. The Bald Eagle Search (BES) algorithm [39] simulates the hunting strategy of bald eagles, and it also belongs to the swarm-based group. The Flow Direction Algorithm (FDA) [40] models the way water flows through terrains and is

classified as physics based. The Gradient-Based Optimizer (GBO) [41] combines mathematical modeling and gradient estimation, making it suitable for the physics-inspired category. Similarly, the Generalized Normal Distribution Optimization (GNDO) [42] uses probabilistic modeling and is placed under evolution-based methods. The Weighted Mean of Vectors (INFO) algorithm [43] utilizes a weighted vector approach for exploitation and exploration and fits well within the evolution-based category. The Marine Predator Algorithm (MPA) [44] mimics the hunting behavior of marine predators, and it is a classic example of swarm intelligence-based optimization. Lastly, the physics-based Runge-Kutta Optimization (RKO) applies Runge-Kutta numerical methods to solve the optimal power flow problem [45]. By selecting algorithms from various backgrounds—biological, physical, mathematical, and behavioral—the study aims to perform a fair and comprehensive comparison of performance across different algorithmic strategies. This diversity also helps examine how different inspiration mechanisms affect results in complex power distribution problems.

The main aim of this research is to determine the algorithms that most effectively achieve multiple goals simultaneously, including minimizing power loss, improving voltage profiles, and reducing unbalanced indices. By applying these algorithms to realistic UPDN models, valuable insights can be provided for network operators and researchers in selecting the most suitable algorithms for specific reconfiguration scenarios. The key contributions of this paper are:

1. A comprehensive analysis of the RecPrb in an unbalanced 123-Bus test system, considering voltage profile improvement, power loss reduction, and minimization of unbalanced indices.
2. A comprehensive and detailed study on the minimization of VUI and CUI in unbalanced PDNs through reconfiguration. This represents the most extensive and in-depth analysis of this topic to date, providing valuable insights into optimizing three-phase unbalanced power systems.
3. Three distinct scenarios are investigated: (a) Scenario 1 focuses on simultaneous power loss minimization and voltage profile improvement. (b) Scenario 2 addresses the minimization of current and voltage unbalanced indices under various operational cases. (c) Scenario 3 implements a multi-objective optimization approach using Pareto front analysis to simultaneously optimize VUI, active power loss, and CUI.
4. Unlike previous studies, this work maintains all components including voltage regulators, capacitor banks, and transformers in the 123-Bus UPDN, ensuring more practical and applicable results.
5. An extensive comparative study of twelve metaheuristic algorithms for solving the RecPrb in UPDNs.
6. A rigorous statistical analysis is performed to determine the most efficient algorithm for solving the RecPrb in the 123-Bus UPDN, employing multiple performance metrics and comparative techniques.
7. Based on the statistical analysis, the AHA is identified as the top-performing algorithm for UPDN reconfiguration problems. Subsequently, AHA is applied to tackle a multi-objective optimization challenge in the 123-Bus UPDN, simultaneously minimizing power losses and unbalanced indices while improving the voltage profile.

The remainder of this paper is structured as follows: Section 2 presents the formulation and constraints of the problem. Section 3 introduces the AHA, which has demonstrated particularly effective results in 123-Bus UPDNs. Section 4 details the 123-Bus distribution test system. Section 5 outlines the various scenarios implemented, discusses the different cases examined under each scenario, and analyzes the results. Finally, the conclusion summarizes the key findings of the paper and suggests potential avenues for further research.

2 Formulization and Constraints

In the optimization of power distribution systems, it is crucial to establish a clear mathematical framework that encompasses both the system's structural requirements and operational limitations. This

section outlines the formulation of the network's radial structure and the various constraints that govern the system's operation. By defining these elements, a robust foundation is created for the subsequent optimization processes aimed at reducing power losses and improving voltage and current balance.

2.1 Radiality

To ensure the reliability and simplicity of the PDN, maintaining its radial structure is crucial. Radial networks, where power flows unidirectionally from substations to consumers, are favored due to their straightforward design and ease of fault isolation and protection device placement [33]. To verify radiality, an incidence matrix B_{nxm} is constructed, where the rows correspond to the branches and the columns correspond to the nodes (buses). The elements of this matrix, b_{ij}, are defined as follows in Eq. (1):

$$B = \begin{cases} b_{ij} = 0, & \text{if branch i is not connected to node j} \\ b_{ij} = 1, & \text{if branch i exist node j} \\ b_{ij} = -1, & \text{if branch i enters node j} \end{cases} \tag{1}$$

Once B is formed, a reference node is selected and removed from the matrix, resulting in a modified incidence matrix B′. In a radial network, the number of nodes is one more than the number of branches. Hence, B′ becomes a square matrix. To check for radiality, the determinant of B′ is calculated. If the determinant is either +1 or −1, the network is radial. Otherwise, the network is either not radial, or one or more nodes are disconnected [33].

2.2 Constraints

The operation of a power distribution network is subject to numerous physical and operational constraints that ensure system stability, reliability, and safety. These constraints encompass various aspects of the network, including voltage levels, current capacities, equipment limitations, and power balance requirements. By explicitly defining these constraints, the boundaries within which the optimization algorithms must operate are clearly established, ensuring that any proposed network reconfiguration remains technically feasible and compliant with operational standards.

- The voltage levels at each bus must remain within specified limits to ensure system stability and reliability. This is expressed as in Eq. (2):

$$V_{i,\phi}^{\min} \le V_{i,\phi} \le V_{i,\phi}^{\max} \qquad \forall \phi \in \{a, b, c\}, \forall i \in \text{Buses} \tag{2}$$

  where $V_{i,\phi}^{min}$ and $V_{i,\phi}^{max}$ are the permissible minimum and maximum voltages at bus i for phase ϕ. For clarity, additional constraints specify acceptable voltage ranges for bus and feeder voltages. Typically, the bus voltage range is ±10%, while the feeder voltage range is ±5%.
- The current flowing through each branch must not exceed the maximum allowable current as in Eq. (3):

$$I_{i,\phi} \le I_{i,\phi}^{\max} \qquad \forall \phi \in \{a, b, c\}, \qquad \forall i \in \text{Branches} \tag{3}$$

  where $I_{i,\phi}$ is the current in branch i for phase ϕ and $I_{i,\phi}^{max}$ is the maximum allowable current for branch i for phase ϕ.
- Voltage regulators must maintain their tap positions within limits as in Eq. (4):

$$Tap_{i,\phi}^{\min} \le Tap_{i,\phi} \le Tap_{i,\phi}^{\max} \qquad \forall \phi \in \{a, b, c\}, \forall i \in \text{Regulators} \tag{4}$$

- Additionally, the voltage at the tap position must be within acceptable limits as in Eq. (5):

$$V_{i,\phi,Tap}^{min} \leq V_{i,\phi,Tap} \leq V_{i,\phi,Tap}^{max} \qquad \forall \phi \in \{a, b, c\} \tag{5}$$

- The power balance equations ensure that the total generated power matches the total load and losses in the system as in Eq. (6):

$$\sum_{i=1}^{N_{Gen}} P_{i,\phi}^{Gen} = \sum_{i=1}^{N_{Load}} P_{i,\phi}^{Load} + \sum_{i=1}^{N_{Branch}} P_{i,\phi}^{Loss} + \sum P_{i,Equipment}^{Loss} \qquad \forall \phi \in \{a, b, c\} \tag{6}$$

where $P_{i,\phi}^{Gen}$, $P_{i,\phi}^{Load}$, and $P_{i,\phi}^{Loss}$ represent the generated, load, and loss power for phases *a, b*, and *c* at bus *i*. $P_{i,Equipment}^{Loss}$ denotes the total equipment losses in the system such as transformers, voltage regulators and similar equipment.

- Capacitor banks must operate within their specified reactive power limits as in Eq. (7):

$$\theta_{i,\phi,cap}^{min} \leq \theta_{i,\phi,cap} \leq \theta_{i,\phi,cap}^{max} \quad \forall \phi \in \{a, b, c\}, \quad \forall i \in \text{Buses} \tag{7}$$

- The transformers must operate within their specified reactance limits as in Eq. (8):

$$X_{i,\phi}^{trf_{min}} \leq X_{i,\phi}^{trf} \leq X_{i,\phi}^{trf_{max}} \quad \forall \phi \in \{a, b, c\}, \forall i \in \text{Transformers} \tag{8}$$

- The apparent power flow on any line must be less than the maximum permissible limit to ensure line security as in Eq. (9):

$$S_{i,\phi,line} \leq S_{i,\phi,line}^{max} \qquad \forall \phi \in \{a, b, c\}, \forall i \in \text{Lines} \tag{9}$$

2.3 Objective Functions

The optimization study focuses on three primary objectives: minimization of active power losses, reduction of voltage unbalance, and mitigation of current unbalance. These objectives are critical for enhancing the overall efficiency and performance of PDNs. This section presents the mathematical formulations of these objective functions, providing a quantitative basis for evaluating various network configurations. The formulation begins with power loss minimization, followed by the definitions of CUI and VUI. These formulations serve as the foundation for the multi-objective optimization approach employed in this study.

2.3.1 Minimizing Power Loss as the Objective

The primary objective in reconfiguring power distribution networks is to identify the network topology that minimizes active power loss. The active power loss (P_L) in a three-phase PDN with N_{branch} branches is calculated as in Eq. (10):

$$P_L = \sum_{i=1}^{N_{Branch}} \sum_{\phi \in \{a,b,c\}} R_{i,\phi} \left| I_{i,\phi} \right|^2 \tag{10}$$

where $R_{i,\phi}$ denotes the resistance of branch i for phase ϕ, $I_{i,\phi}$ is the current flowing through branch i for phase ϕ, and $\phi \in \{a, b, c\}$ represents the three phases of the system. This formulation explicitly accounts for the contribution of each phase to the total system losses.

2.3.2 Voltage and Current Unbalanced Indices

Voltage and current unbalance in power distribution networks can lead to various issues, such as equipment overheating, increased system losses, and reduced power quality. Specifically, the disparity in current values flowing through each phase conductor causes an unbalanced state, which results in increased power losses [46]. The concept of voltage unbalance factor varies across different standards and communities. However, a commonly accepted definition involves the ratio of the negative-sequence component to the positive-sequence component of the voltages [30]. To quantify the unbalance in power distribution networks, the unbalance index (UI) can be calculated using Eq. (11) as follows:

$$\mathrm{UI}\,(\%) = \left(\frac{|\mathrm{X_{neg}}|}{|\mathrm{X_{pos}}|}\right) \times 100 \tag{11}$$

where X_{neg} and X_{pos} denote the negative sequence component and the positive sequence component, respectively.

Various methods have been proposed by researchers to mitigate voltage and current unbalance in distribution networks. One approach is the implementation of active power electronics-based solutions, such as dynamic voltage restorers and unified power quality conditioners, which compensate for voltage and current imbalances [47]. Another strategy involves network reconfiguration, which modifies the topological structure of the distribution network by adjusting switches to balance the load across the phases [33]. Additionally, integrating distributed generation units, like solar photovoltaic systems, can help reduce voltage and current unbalance by providing local generation support.

3 Artificial Hummingbird Algorithm

The artificial hummingbird algorithm (AHA) is a recently introduced bio-inspired optimization method developed by Zhao et al. [37]. It is inspired by the exceptional flight abilities and smart foraging techniques of hummingbirds to collect nectar. A key step in the AHA involves the selection of sources of food, where the hummingbird chooses a suitable food source determined by factors such as the nectar content of each flower, nectar quality, nectar replenishment rate, and the time elapsed since the last visit to a flower. In the AHA, each food source serves as a solution vector, where the nectar replenishment rate signifies the fitness value. Consequently, a greater nectar replenishment rate corresponds to an improved fitness value.

In the AHA, every hummingbird is allocated to a specific food source, meaning that the food source and the locations of the hummingbird coincide. The algorithm allows for the storage of information regarding the nectar replenishment rate, the location of the food source, and sharing of this information with other members of the population. Additionally, each hummingbird keeps track of how long it has been since a particular food source was last visited. This information is recorded in a schedule called the visit table, which tracks the frequency of visits to each food source allocated to a hummingbird. The hummingbird prioritizes food sources with high visitation levels. When seeking nectar, hummingbirds tend to visit the food source with the highest nectar refilling rate among those with the same highest visitation level. Therefore, each hummingbird can assess its designated food source using the visitation table, which is continuously revised throughout the iterative process. Hummingbirds exhibit three distinct foraging behaviors: guided, territorial, and migrating. To mimic these behaviors in the algorithm, an initial population of hummingbirds is randomly created within the bounds of the search space, facilitating the construction of a model that emulates hummingbird behavior. In Eq. (12), the position of the i^{th} food source is represented by $\mathrm{p_i}$, while $\mathrm{b_{low}}$ and $\mathrm{b_{up}}$ indicate the lower and upper bounds of the search space for the given problem. Additionally, the variable "rand" represents a random number within the range of [0, 1].

$$p_i = b_{low} + rand * \left(b_{up} - b_{low}\right), \qquad i = 1, 2, 3, \ldots, n \tag{12}$$

To initialize the food source visit table (ToV), the following approach can be employed as in Eq. (13):

$$ToV_{i,j} = \begin{cases} 0 & \text{in the case of } i \neq j \\ null & \text{in the case of } i = j \end{cases} \qquad i, j = 1, 2, 3, \ldots, n \tag{13}$$

3.1 Directed Foraging

Each hummingbird has a tendency to visit the food source with the highest volume of nectar. This implies that the desired food source should have a high rate of nectar refilling and should not have been recently visited by other hummingbirds for a long period of time. Consequently, the hummingbird identifies the food sources with the highest levels of visitation and designates the one with the greatest nectar replenishment rate as its target. Subsequently, the hummingbird flies towards this location to consume the food. The AHA approach incorporates three flight skills inspired by hummingbirds: omnidirectional, diagonal, and axial flights. The choice and control of the flight skill are determined by the direction-switching vector, which determines whether one or multiple directions are explored in the a-dimensional search space. During the axial flight, the hummingbird moves along the coordinate axis, whereas in the diagonal flight, it moves from one corner of the search space to the opposite corner. The axial flight can be mathematically represented as in Eq. (14):

$$A_i = \begin{cases} 1 & \text{if } i = randi\left([1, a]\right) \\ 0 & \text{else} \end{cases} \qquad i = 1, 2, 3, \ldots, a \tag{14}$$

The diagonal flight formulation is given Eq. (15):

$$A_i = \begin{cases} 1, & i = D(j), j \in [1, k], D = randperm\ (k), k \in [2, r_1.(a-2)] + 1 \\ 0, & \text{else} \end{cases} \quad i = 1, 2, \ldots, a \tag{15}$$

The omnidirectional flight can be expressed as in Eq. (16) as follows:

$$A_i = 1, \qquad i = 1, 2, 3, \ldots, a \tag{16}$$

In order to achieve these flight capabilities, certain mechanisms are employed. The vector randi (1, a) consists of randomly generated numbers ranging from 1 to a, randperm (k) generates random permutations within the range of 1 to k, and r1 represents a random number within the interval of [0, 1]. Leveraging these flight capabilities, the hummingbird is able to visit the desired food source, leading to the identification of a potential source. Consequently, the food source is updated based on a combination of the previous and target food sources. This process of guided foraging can be described using the following representation, as outlined in Eq. (17):

$$v_i^{(t+1)} = x_{i,target}^{(t)} + \alpha D \left(x_i^{(t)} - x_{i,target}^{(t)}\right), \quad \alpha \sim N(0, 1) \tag{17}$$

In the context of the algorithm, several variables play a crucial role. Here, x_i^t represents the food source with index i at iteration t, $x_{i,target}^t$ refers to the target food source that the i^{th} hummingbird intends to visit at iteration t, and α is a guided factor that follows a normal distribution as N(0, 1). Additionally, alfa is a

guided factor that conforms to the normal distribution. The position of the food source is adjusted using the Eq. (18):

$$x_i^{(t+1)} = \begin{cases} x_i^{(t)}, & f(x_i^{(t)}) \le f(v_i^{(t+1)}) \\ v_i^{(t+1)}, & f(x_i^{(t)}) > f(v_i^{(t+1)}) \end{cases} \tag{18}$$

In the equation mentioned, f represents the fitness value associated with the food source.

3.2 Territorial Foraging

Following the consumption of flower nectar, the hummingbird engages in a search for new food sources by moving to neighboring regions. It is possible that these food sources may offer superior benefits compared to the current one. The local area search process associated with territorial foraging can be expressed in Eq. (19) as follows:

$$v_i^{(t+1)} = x_i^{(t)} + bAx_i^{(t)}, \quad b \sim N(0,1) \tag{19}$$

where b denotes the territorial factor that adheres to a normal distribution.

3.3 Migration-Based Foraging

In situations where regions commonly frequented by hummingbirds are often deficient in adequate food resources, the hummingbirds tend to migrate towards distant food sources to find nourishment. The AHA algorithm incorporates a migration factor that governs this behavior. If the iteration count surpasses the predefined migration factor value, a hummingbird located at a food source with the lowest nectar replenishment rate will relocate to a new source. This new source is randomly generated within the entire search space, representing an alternative option for the hummingbird. During this migration process, the hummingbird abandons the old source and settles at the new source. Consequently, the visitation schedule is updated to reflect this change. The migration of a hummingbird from a source with a suboptimal nectar refill rate to a new source can be accomplished using the following expression in Eq. (20):

$$x_{worst}^{(t+1)} = b_{low} + rand * (b_{up} - b_{low}) \tag{20}$$

To determine the new position for the source with the lowest nectar replenishment rate at iteration $(t+1)$, Eq. (20) is utilized, where x_{worst}^{t+1} signifies the location of the food source with the lowest nectar refill rate at the given iteration, b_{low} and b_{up} indicate the lower and upper bounds of the search space, and *rand* represents a random number in the range $[0, 1]$.

4 Power System Simulation Platform

In this section, the simulation platform used for the analysis of the UPDN is presented. The platform was developed entirely using the MATLAB environment, incorporating the well-established backward-forward sweep (BFS) method for power flow calculations. This method was specifically chosen for its superior convergence properties and computational efficiency when applied to radial distribution networks with unbalanced loading conditions. The platform enables the accurate modeling of all system components including lines, transformers, voltage regulators, capacitor banks, and various load types, providing a robust foundation for the assessment of network reconfiguration strategies.

4.1 Simulation Platform Architecture

The simulation platform consists of four integrated modules designed to handle specific aspects of the UPDN analysis:

i. **Network Topology Manager:** Controls network configuration data structures, manages switch operations (both sectionalizing and tie switches), and maintains radiality constraints using the determinant-based approach described in Section 2.1.
ii. **Component Modeling Module:** Implements detailed models of distribution system components according to IEEE standards, including transformers, voltage regulators, capacitor banks, various line configurations, and other components.
iii. **Three-Phase Unbalanced Power Flow Solver:** Employs the backward-forward sweep algorithm optimized for radial unbalanced systems, accounting for mutual phase couplings and asymmetrical loading conditions.
iv. **Performance Evaluation Module:** Calculates active power losses, voltage profiles, and power quality indices (VUI and CUI) based on the mathematical formulations in Sections 2.2 and 2.3.

These modules interact within an object-oriented framework, facilitating the efficient integration of metaheuristic algorithms for network reconfiguration studies.

4.2 Implementation of the Unbalanced Three-Phase Backward-Forward Sweep Load Flow (BFLF) Algorithm

The backbone of the simulation platform is the implementation of an unbalanced three-phase backward-forward sweep (UBFS/UBFLF) load flow algorithm. This method was selected for its robust convergence characteristics when applied to radial distribution networks with high R/X ratios and significant phase imbalances. The UBFLF algorithm avoids the computational challenges often encountered with traditional Newton-Raphson methods in distribution systems, such as ill-conditioned Jacobian matrices and convergence difficulties under highly unbalanced conditions. The implementation of the UBFLF algorithm is specifically tailored to handle the complexities of the IEEE 123-Bus test system, including its diverse line configurations, multiple load types, and various system parts such as capacitor banks, transformers, and voltage regulators. The algorithm accurately accounts for mutual coupling between phases, which is essential for the correct representation of unbalanced three-phase systems. Fig. 1 illustrates the three-phase power distribution line segment model used in the implementation.

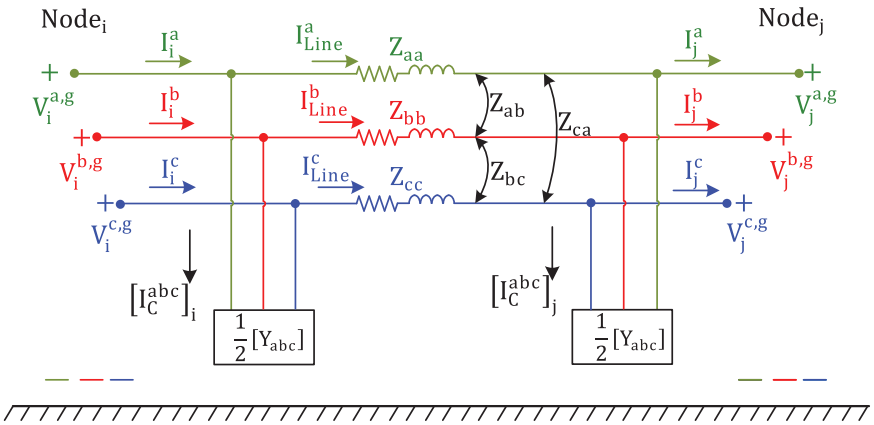

Figure 1: Three-phase power distribution line segment model [31]

The UBFLF method implementation follows a systematic four-step process:

4.2.1 Initialization

Set all node voltages to nominal values (1.0 p.u.) and compute the initial branch currents from the specified loads.

4.2.2 Backward Sweep

Beginning at the terminal nodes and proceeding upstream toward the substation, branch currents are updated according to Kirchhoff's Current Law (KCL) as given in Eq. (21):

$$I_{ij}^{abc} = \sum_{k \epsilon Dj} I_{jk}^{abc} + Y_{j}^{abc} \times V_{j}^{abc} \tag{21}$$

where I_{ij}^{abc} represents the three-phase current flowing from node i to node j, D_j is the set of nodes directly connected to node j, Y_j^{abc} is the three-phase admittance matrix at node j, and V_j^{abc} is the three-phase voltage at node j.

4.2.3 Forward Sweep

Starting from the substation and moving toward the terminal nodes, update node voltages using the formula presented in Eq. (22):

$$V_{j}^{abc} = V_{i}^{abc} - Z_{ij}^{abc} \times I_{ij}^{abc} \tag{22}$$

where Z_{ij}^{abc} is the three-phase impedance matrix of the branch connecting nodes i and j.

4.2.4 Convergence Check

Compute the maximum voltage mismatch between consecutive iterations as defined in Eq. (23):

$$\Delta V_{max} = \max_{j,abc} \left| V_{j}^{abc}(k) - V_{j}^{abc}(k-1) \right| \tag{23}$$

If $\Delta V_{max} < \varepsilon$ (where $\varepsilon = 10^{-6}$ p.u.), the process terminates; otherwise, it returns to the backward sweep step.

The algorithm is enhanced with acceleration techniques to handle systems with voltage regulators, transformers, and capacitor banks. For voltage regulators, tap positions are updated after each forward sweep based on the voltage regulation constraints. Special care is taken to handle the phase shifts introduced by different transformer connections (Δ-Y, Y-Δ, etc.) by appropriately modifying the current and voltage values during the sweeps.

4.3 Modeling Approaches for Unbalanced Systems

The unbalanced nature of distribution systems requires specialized modeling approaches that consider phase imbalances, mutual couplings, and different load types:

4.3.1 Line Modeling

Three-phase lines are represented using phase impedance matrices as shown in Eq. (24):

$$Z_{abc} = \begin{bmatrix} Z_{aa} & Z_{ab} & Z_{ac} \\ Z_{ba} & Z_{bb} & Z_{bc} \\ Z_{ca} & Z_{cb} & Z_{cc} \end{bmatrix} \tag{24}$$

Diagonal elements represent self-impedances of each phase, while off-diagonal elements represent mutual impedances between phases. The IEEE 123-Bus test system includes 11 different overhead and 1 underground line configurations, each with specific impedance matrices as defined in the test system specifications.

4.3.2 Load Modeling

Load models were implemented to accurately represent diverse consumption patterns:

a. Constant Impedance (Z): Represents loads whose power consumption changes with the square of the voltage magnitude, typical for resistive heating elements and incandescent lighting, as expressed in Eq. (25):

$$S_{abc} = S_0^{abc} \times \left(\frac{|V_{abc}|}{|V_0|} \right)^2 \tag{25}$$

b. Constant Current (I): Characterizes loads whose power consumption varies linearly with voltage magnitude, commonly found in certain electronic devices and small motors, as shown in Eq. (26):

$$S_{abc} = S_0^{abc} \times \left(\frac{|V_{abc}|}{|V_0|} \right) \tag{26}$$

c. Constant Power (PQ): Maintains constant complex power (consumption) regardless of voltage variations, such as electronically controlled loads and modern variable-speed drives, as defined in Eq. (27):

$$S_{abc} = S_0^{abc} \tag{27}$$

d. Composite loads: Composite loads are implemented as combinations of constant impedance, constant current, and constant power models in both wye (Y) and delta (Δ) configurations. These load models are mathematically represented during the backward sweep process according to Eq. (28):

$$I_{load}^{abc} = \text{conj}\left(\frac{S_{load}^{abc}}{V^{abc}} \right) \times f\left(\frac{|V^{abc}|}{|V_0|} \right) \tag{28}$$

where I_{load}^{abc} denotes the three-phase load current vector, S_{load}^{abc} denotes the three-phase complex power demand, V^{abc} is the three-phase voltage vector at the bus, and $f(\cdot)$ is a function characterizing the voltage dependency according to the load type. The voltage dependency function varies based on the load model: quadratic for constant impedance loads, linear for constant current loads, and inverse for constant power loads.

e. Distributed load: Loads uniformly distributed along line segments, approximated by splitting the load between two connection points. Mathematically represented as in Eq. (29):

$$\begin{aligned} S_i &= k_i \times S_{total} \\ S_j &= (1 - k_i) \times S_{total} \end{aligned} \tag{29}$$

where S_{total} is the total distributed load, S_i and S_j are the portions allocated to connection points i and j, respectively, and k_i is the distribution factor (typically 0.5 for uniform distribution).

4.3.3 Transformer Modeling

Multiple transformer connections were modeled using appropriate admittance matrices and phase shifts. In the IEEE 123-Bus test system, two transformers are included:

- A substation transformer (Delta-Wye grounded, 5000 kVA, 115/4.16 kV with R=1%, X=8%)
- A distribution transformer (XFM-1, Delta-Delta, 150 kVA, 4.16/0.480 kV with R=1.27%, X=2.72%).

a. For a Δ-Y grounded transformer like the substation transformer, the correlation between primary (p) and secondary (s) currents is given by Eq. (30):

$$\begin{bmatrix} I_a^p \\ I_b^p \\ I_c^p \end{bmatrix} = \begin{bmatrix} 1 & -1 & 0 \\ 0 & 1 & -1 \\ -1 & 0 & 1 \end{bmatrix} \begin{bmatrix} I_a^s \\ I_b^s \\ I_c^s \end{bmatrix} \times \left(\frac{1}{\sqrt{3}}\right) \times \alpha \tag{30}$$

b. For a Δ-Δ transformer like XFM-1, both primary and secondary currents maintain the same phase relationship but are scaled by the turns ratio as in Eq. (31):

$$\begin{bmatrix} I_a^p \\ I_b^p \\ I_c^p \end{bmatrix} = \begin{bmatrix} 1 & 0 & 0 \\ 0 & 1 & 0 \\ 0 & 0 & 1 \end{bmatrix} \begin{bmatrix} I_a^s \\ I_b^s \\ I_c^s \end{bmatrix} \times \alpha \tag{31}$$

where α is the turns ratio ($\alpha = \frac{V_p}{V_s} = \frac{4.16}{0.48} = 8.67$ for XFM-1). The transformer impedances are incorporated into the network model by converting the per-unit impedance values to actual impedances.

4.3.4 Voltage Regulator Modeling

Voltage regulators were modeled as autotransformers with adjustable tap positions in 32 steps (±16 steps of 0.00625 p.u. each). Mathematically, the voltage interrelation between the primary (p) and secondary (s) sides can be expressed as in Eq. (32):

$$V_s^{abc} = \left(1 + \Delta T^{abc}\right) \times V_p^{abc} \tag{32}$$

where V_s^{abc} and V_p^{abc} are the three-phase voltage vectors on the secondary and primary sides, respectively, and ΔT^{abc} is the tap position matrix as defined in Eq. (33):

$$\Delta T^{abc} = \begin{bmatrix} T_a & 0 & 0 \\ 0 & T_b & 0 \\ 0 & 0 & T_c \end{bmatrix} \tag{33}$$

with $T_\varphi = n_\varphi \times 0.00625$ p.u., where $n_\varphi \in \{-16, -15, \ldots, 0, \ldots, 15, 16\}$ is the tap position for phase $\varphi \in \{a, b, c\}$.

4.4 123-Node Distribution Test System Details

The IEEE 123-Bus unbalanced test feeder has multiple distinctive characteristics that are thoroughly elaborated in reference [48], setting it apart from other test feeders. Fig. 2 illustrates this PDN test system

with its significant operational parameters. The system operates at a nominal voltage of 4.16 kV with a total active power of 3490 kW and reactive power of 1920 kVAr. According to reference [48], the initial case reports total active and reactive power losses of 95.611 kW + j193.727 kVAr, respectively. The test infrastructure incorporates 12 switches strategically positioned throughout the network, comprising overhead line segments in 11 distinct configurations and underground line segments in a single configuration, with most segments featuring multiple phases. Furthermore, the system includes four capacitor banks, where three are assigned to single-phase buses, with a single component connected to a three-phase bus. Additionally, four voltage regulators with varying connection topologies are integrated into the system to maintain voltage stability.

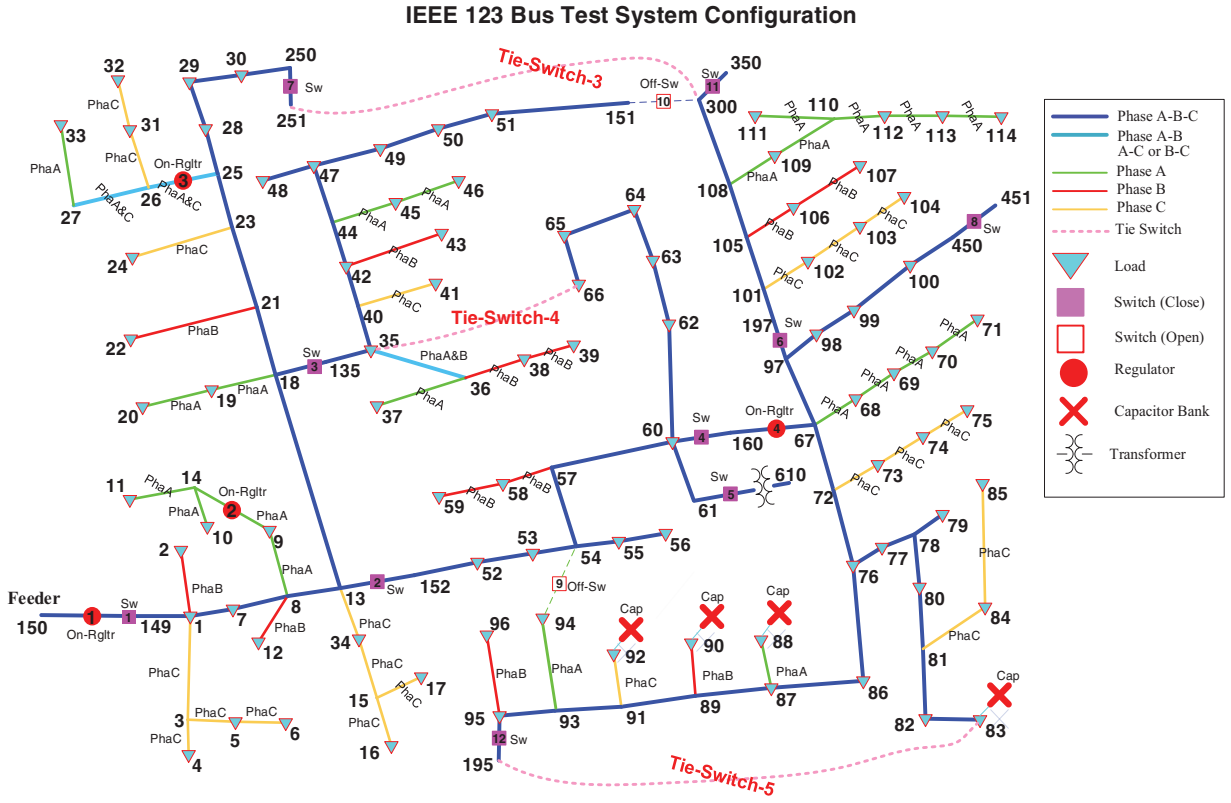

Figure 2: 123-Bus PDN test system topology showing the distribution of buses, switches, and regulatory elements

In the 123-Bus test system, 12 switches were placed at various locations. However, within this section, it is presumed that switches are installed on every branch to increase the search space. Additionally, the system is enhanced by incorporating 3 TSs, as detailed in Table 1.

Table 1: The length and locations of additional tie-switches

Tie-switch no.	From bus	To bus	Length (Feet)	Line configuration no.
3	251	300	2000	1 (3~overhead line)
4	35	66	750	12 (3~underground line)
5	83	195	1500	2 (3~overhead line)

The rationale for adding TSs includes: (a) reducing the number of customers affected during faults, (b) adding complexity to the system to assess the algorithms' performance, (c) improvement of VUI and CUI, and (d) reducing active power loss. The results incorporating additional data are explained in Section 5. In this study, the bus numbering system provided by IEEE-PES follows a sequential order up to bus 114; however, after bus 135, the numbering is no longer in ascending order, with bus numbers such as 135, 149, 150, and so on.

To facilitate a clearer and more structured presentation in this paper, these bus numbers have been renumbered in ascending order, starting from 115. For example, bus number 135 is now referred to as 115, and bus number 149 as 116. This renumbering ensures consistency and ease of interpretation, particularly in graphical and tabular representations of the power distribution network. The renumbered bus information is provided in Table 2, where the corresponding IEEE-PES bus numbers and their new assignments are listed for reference.

Table 2: Renumbering of IEEE-PES bus numbers for graphical representation

Bus no. in graph	**115**	**116**	**117**	**118**	**119**	**120**	**121**	**122**	**123**	**124**	**125**	**126**	**127**	**128**	**129**
IEEE-PES Bus No.	135	149	150	151	152	160	195	197	250	251	300	350	450	451	610

4.5 Validation of the Simulation Platform Using the IEEE-123 Bus System

To ensure the accuracy and reliability of the developed simulation platform, comprehensive validation was conducted through detailed comparisons with established power system analysis tools and reference data. This validation process is essential to confirm that the platform correctly models the complex dynamics of unbalanced power distribution networks before proceeding with reconfiguration studies.

4.5.1 Relative Error Assessment

The quality of the simulation results was evaluated by comparing the output of the developed MATLAB implementation with reference values from the IEEE-123 Bus system. For quantitative evaluation, the Relative Error (RE) for both voltage and current values was calculated using Eq. (34):

$$V_{RE} = \left| \frac{V^{abc}_{WMs} - V^{abc}_{IEEE}}{V^{abc}_{IEEE}} \right| \text{ and } I_{RE} = \left| \frac{I^{abc}_{WMs} - I^{abc}_{IEEE}}{I^{abc}_{IEEE}} \right| \tag{34}$$

where V^{abc}_{WMs} and I^{abc}_{WMs} represent the three-phase voltage and current vectors obtained from the developed MATLAB implementation, while V^{abc}_{IEEE} and I^{abc}_{IEEE} are the corresponding reference values from the IEEE-123 Bus system documentation. Figs. 3 and 4 illustrate the distribution of these relative errors across the network. The Current Relative Error distribution (Fig. 3) shows the deviation between calculated and reference current values at each branch, while the Voltage Relative Error distribution (Fig. 4) demonstrates the accuracy of voltage calculations at each bus in the system. As evident from these figures, the developed simulation platform demonstrates excellent agreement with the reference values. The maximum relative errors remain consistently below 10^{-3}, which is well within acceptable engineering tolerance for power system simulations.

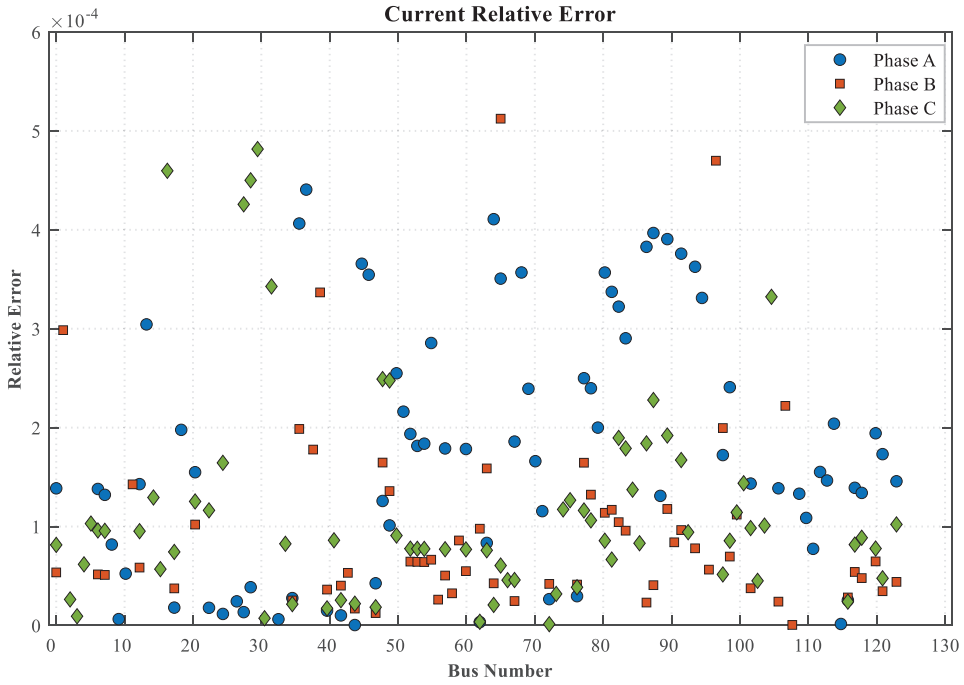

Figure 3: Current relative error between MATLAB implementation and reference values [31,33]

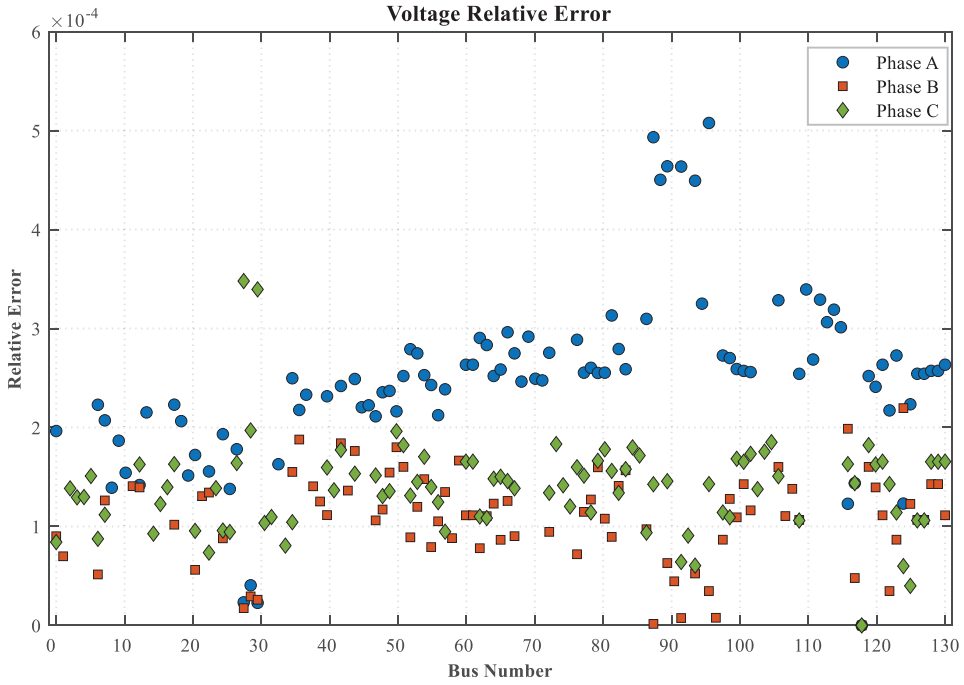

Figure 4: Voltage relative error between MATLAB implementation and reference values [31,33]

4.5.2 Comparative Analysis Using Industry-Standard Tools

To further validate the simulation platform, a comparative analysis was conducted between the results obtained from the developed code (labeled as "WMs") and three established reference sources: the official

IEEE-PES test case results, OpenDSS simulation software, and MATLAB/Simulink. Table 3 presents this comparison across key system parameters including reactive and active power losses, apparent power losses, and voltage extremes.

Table 3: Performance comparison between IEEE-PES, OpenDSS, MATLAB/Simulink, and the proposed method (WMs) for the IEEE 123-Bus Test System under initial conditions [31]

	Developed code (WMs)	IEEE-PES test case	MATLAB simulink	Open-DSS software
$\mathbf{P_{loss}}$ (kW)	95.5939	95.611	95.5198	95.2828
$\mathbf{Q_{loss}}$ (kVAr)	192.4649	193.727	192.3978	190.9900
$\mathbf{S_{loss}}$ (kVA)	214.8975	216.036	214.8044	213.4385
$\mathbf{V_{min}}$ (p.u.) Bus No., Phase	0.9858, Bus 65, Phase A	0.9856, Bus 65, Phase A	0.9858, Bus 65, Phase A	0.9858, Bus 65, Phase A
$\mathbf{V_{max}}$ (p.u.) Bus No., Phase	1.0437, Bus 149, Phase A, B, C	1.0438, Bus 149, Phase B, C	1.0439, Bus 83, Phase A	1.0437, Bus 149, Phase A, B, C

The results in Table 3 show that the developed simulation platform (WMs) shows excellent agreement with the official IEEE-PES test case results, with deviations below 0.02% for active power losses and 0.003% for minimum voltage values. The minor differences observed across all tools can be attributed to slight variations in component modeling approaches, numerical solution methods, and precision settings in the different software environments. This validation confirms the high accuracy of the simulation platform, providing a reliable foundation for the comprehensive analysis of reconfiguration strategies in UPDNs presented in subsequent sections. The platform's ability to accurately model unbalanced three-phase systems with complex components such as capacitor banks, transformers, and voltage regulators, while maintaining computational efficiency, makes it particularly suitable for the extensive statistical analysis of multiple metaheuristic algorithms conducted in this study.

5 Scenarios & Results

In this study, twelve algorithms from the literature, used to solve the RecPrb, are reprogrammed and reapplied. Nine out of the twelve algorithms have not been applied to the RecPrb of unbalanced power distribution systems before. These algorithms are statistically analysed and evaluated using a 123-Bus test system. In the study, each algorithm is executed 500 times independently. The control parameters for all optimization algorithms are selected based on their original implementations presented in the corresponding literature.

For all applied search algorithms, the population size and the number of iterations are set to 100 and 200, respectively, for the 123-Bus networks. This configuration ensures a fair comparison by conducting similar function evaluations [11]. Increasing the iteration count and the size of the population in swarm intelligence (SI) based algorithms is known to result in longer execution (elapsed) times for these algorithms. Hence, in the present study, each algorithm is limited to a maximum of 200 iterations. This study comprises three main parts.

- In scenario I, the fitness function is to minimize the active power loss and improve the voltage magnitude in the PDN. Eq. (10) defines the objective functions used in the process of reconfiguration, while Eqs. (1)–(9) outline the overall constraints of the lines [11]. The performance of all algorithms is evaluated using statistical tests.

- In the second scenario, the fitness function is to enhance power quality by minimizing the CUI and VUI values.
- In the third scenario, the focus is on the multi-objective reconfiguration problem, addressing both power quality (VUI and CUI) and decrease in power loss, derived from a viable Pareto-optimal set. In this context, active power loss, VUI, and CUI are treated as the primary objectives.

The time required for computations varies based on several factors, including the effectiveness of the metaheuristic optimization algorithm, the computer hardware configuration, and the effectiveness of the designed algorithms. For this study, the analyses are executed using MATLAB software on a system featuring an i5-7400T processor operating at 2.40 GHz and 8 GB of RAM.

Fig. 5 presents the flowchart of the optimization approaches implemented in this study. The process begins with system initialization, including network topology and parameter settings. Each metaheuristic algorithm then generates candidate solutions proposing potential network configurations. These configurations are evaluated using the backward-forward sweep load flow solver to compute power losses, voltage profiles, and unbalanced indices. Based on these evaluations, the algorithms iteratively refine their solutions until convergence criteria are met. This systematic approach ensures that all network constraints are properly enforced throughout the reconfiguration process while allowing for fair comparison between different optimization techniques.

5.1 Scenario I: Optimization of Power Distribution Systems for Minimization of Active Power Losses

In the first scenario, an optimization study is conducted to minimize active power losses in the IEEE 123-Bus test system. This study evaluates the performance of twelve metaheuristic optimization algorithms in addressing the specified objective function. The results of this comprehensive analysis are presented in Table 4.

5.1.1 Performance Analysis of Metaheuristic Algorithms

The experimental setup for all algorithms-maintained consistency across several parameters. To ensure statistical robustness and account for the stochastic nature of metaheuristic algorithms, each algorithm was executed 500 times. Table 4 provides a detailed comparison of the algorithms' performances. It presents the best- and worst-case switch statuses and corresponding power losses for each tested algorithm. Notably, the table also includes the number of times each algorithm achieved the global optimum out of the 500 executions, offering insights into the algorithms' reliability and consistency. The results indicate that several algorithms, including AHA, BES, DE, EO, FDA, GBO, INFO, MPA, RKO, and SMA, consistently achieved the minimum power loss of 83.593 kW in their best-case scenarios. This outcome suggests a high level of effectiveness among these algorithms in identifying optimal network configurations for loss minimization. An analysis of the worst-case scenarios reveals significant variations in the algorithms' robustness. The SMA algorithm demonstrated the highest worst-case power loss at 86.196 kW, representing a 9.8309% reduction from the base case. In contrast, AHA showed the lowest worst-case power loss at 83.72995 kW, maintaining a 12.411% reduction even in its worst performance. This indicates that AHA not only achieves the global optimum frequently but also maintains consistently low power losses across all runs.

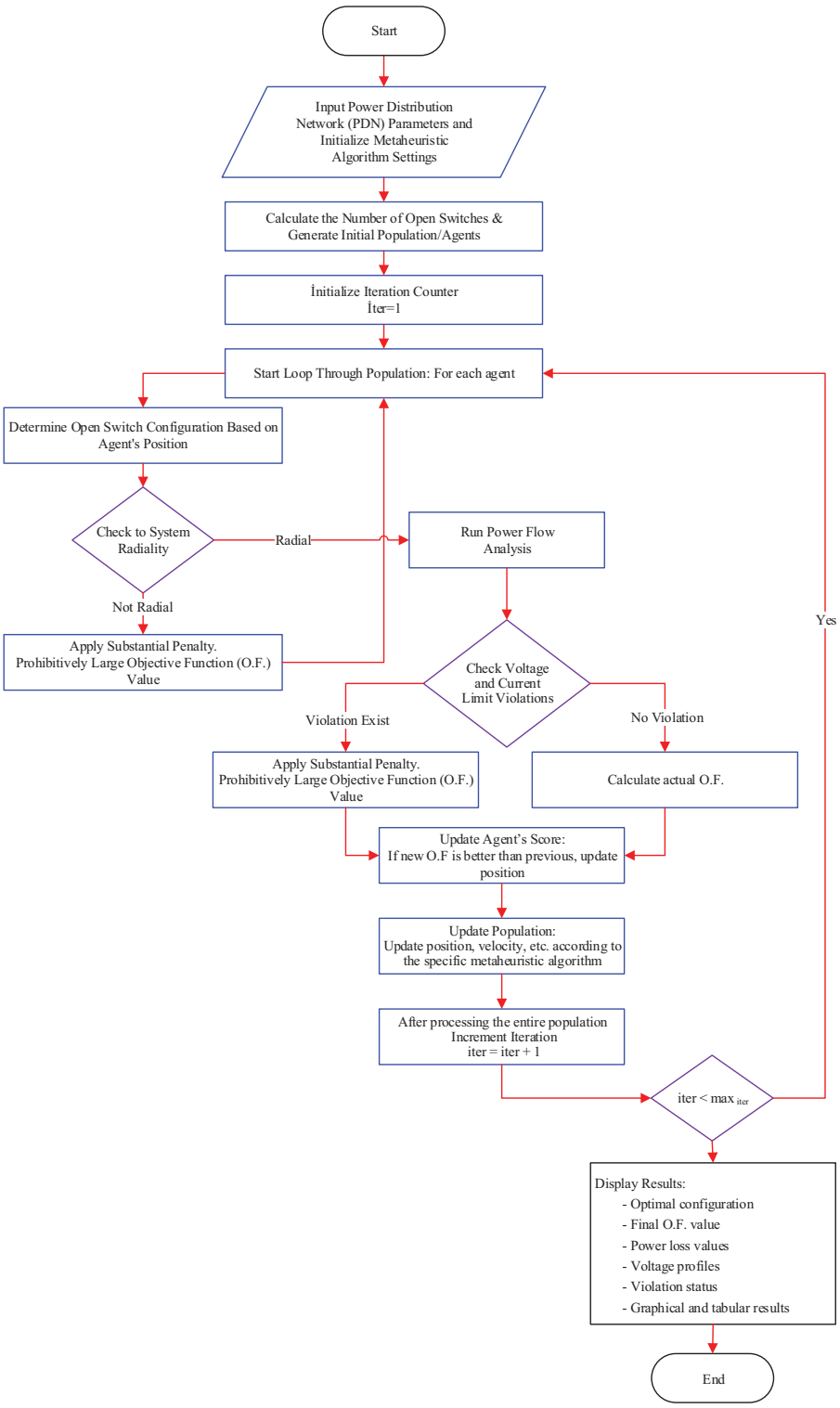

Figure 5: Flowchart of metaheuristic algorithms for PDN reconfiguration

Table 4: Performance comparison of metaheuristic algorithms for power loss minimization in IEEE 123-Bus system

Algorithms name	Best case P_{loss}^{min} (kW)	Worst case P_{loss}^{max} (kW)	Average P_{loss}^{Ave} (kW)	No. of global optima out of 500 times	Open switches (Tie-switches) for best case	Open switches (Tie-switches) for worst case	% Power loss reduction for P_{Loss}^{Best} & P_{Loss}^{Worst}
AHA	83.593	83.72995	83.594	493/500	47–49, 64–65, 72–76, 76–77, 108–300	64–65, 72–76, 76–77, 250–251, 151–300	12.554% (Best) 12.411% (Worst)
AOA	83.731	93.893	86.039	0/500	64–65, 72–76, 76–77, 151–300, 251–300	54–57, 63–64, 101–105, 95–195, 251–300	12.409% (Best) 1.7793% (Worst)
BES	83.593	84.374	83.782	25/500	47–49, 64–65, 72–76, 76–77, 108–300	50–51, 62–63, 72–76, 76–77, 30–250	12.554% (Best) 11.737% (Worst)
DE [26]	83.593	84.554	83.898	4/500	47–49, 64–65, 72–76, 76–77, 108–300	60–62, 72–76, 76–77, 250–251, 151–300	12.554% (Best) 11.549% (Worst)
EO [26]	83.593	84.25	83.774	75/500	47–49, 64–65, 72–76, 76–77, 108–300	29–30, 50–51, 64–65, 67–72, 76–77	12.554% (Best) 11.867% (Worst)
FDA	83.593	85.715	83.83	71/500	47–49, 64–65, 72–76, 76–77, 108–300	72–76, 76–86, 51–151, 97–197, 35–66	12.554% (Best) 10.335% (Worst)
GBO	83.593	84.291	83.714	151/500	47–49, 64–65, 72–76, 76–77, 108–300	64–65, 72–76, 76–86, 30–250, 151–300	12.554% (Best) 11.824% (Worst)
GNDO	83.678	87.662	84.884	0/500	49–50, 64–65, 72–76, 76–77, 108–300	65–66, 72–76, 87–89, 101–105, 251–300	12.465% (Best) 8.2979% (Worst)
INFO	83.593	84.002	83.668	234/500	47–49, 64–65, 72–76, 76–77, 108–300	49–50, 64–65, 67–72, 76–77, 251–300	12.554% (Best) 12.126% (Worst)
MPA	83.593	84.292	83.752	137/500	47–49, 64–65, 72–76, 76–77, 108–300	64–65, 72–76, 76–86, 151–300, 251–300	12.554% (Best) 11.823% (Worst)
RKO	83.593	84.25	83.70	274/500	47–49, 64–65, 72–76, 76–77, 108–300	29–30, 50–51, 64–65, 67–72, 76–77	12.554% (Best) 11.867% (Worst)
SMA [26]	83.593	86.196	83.747	152/500	47–49, 64–65, 72–76, 76–77, 108–300	76–77, 197–101, 60–160, 151–300, 35–66	12.554% (Best) 9.8309% (Worst)

The average power loss values provide further insights into the algorithms' overall performance. AHA exhibited the lowest average power loss at 83.594 kW, nearly identical to its best-case scenario, underscoring its exceptional consistency. Conversely, GNDO showed the highest average power loss at 84.884 kW, suggesting less consistent performance across multiple runs. The narrow range of average power losses (between 83.594 kW and 84.884 kW) among all algorithms indicates that they all perform reasonably well in minimizing power losses, with subtle differences in their consistency and robustness. However, the algorithms exhibited varying levels of robustness, as evidenced by their worst-case performances and the frequency of achieving the global optimum. For instance, AHA reached the global optimum in 493 out of

500 runs, demonstrating exceptional consistency. In contrast, AOA and GNDO did not achieve the global optimum in any of the 500 runs, indicating potential limitations in their application to this specific problem.

5.1.2 Convergence Analysis

The convergence characteristics of the examined algorithms are presented in Table 5, which details the iteration numbers required to reach local or global optima. This data contributes to a deeper comprehension of the computational efficiency of each algorithm. INFO demonstrated the lowest average number of iterations (81.012) to reach convergence, suggesting superior efficiency in this context. Conversely, GNDO required the highest average number of iterations (156.97), indicating a potentially slower convergence rate. The maximum iteration numbers reveal that some algorithms, such as BES, DE, EO, FDA, GBO, and GNDO, utilized the full allocation of 200 iterations in certain runs. This observation suggests that these algorithms might benefit from an increased iteration limit in some cases to potentially improve their solutions. Minimum iteration numbers varied significantly among the algorithms, ranging from 1 (AOA and FDA) to 44 (RKO).

Table 5: Convergence analysis of metaheuristic algorithms for power loss minimization

Algorithms name	Number of iteration for P_{loss}^{min} (kW)		
	Maximum	Minimum	Average
AHA	192	7	120.23
AOA	188	1	143.9
BES	200	10	139.27
DE [26]	200	9	141.71
EO [26]	200	15	123.89
FDA	200	1	115.6
GBO	200	9	124.29
GNDO	200	30	156.97
INFO	164	16	81.012
MPA	188	19	128.77
RKO	177	44	101.36
SMA [26]	182	42	117.88

This variation highlights the diverse search strategies employed by different algorithms and their varying abilities to quickly identify promising solutions in the search space. In conclusion, this comprehensive analysis of twelve metaheuristic optimization algorithms for minimizing active power losses in the IEEE 123-Bus test system reveals significant variations in performance, consistency, and convergence characteristics. While several algorithms demonstrated the ability to achieve the global optimum, their reliability and computational efficiency differed substantially. The analysis of worst-case scenarios and average power losses further highlights the trade-offs between achieving optimal solutions and maintaining consistent performance across multiple runs. These findings provide valuable insights for selecting appropriate algorithms for similar power system optimization problems and highlight areas for potential algorithmic improvements.

5.1.3 Statistical Assessment of the Algorithms' Performance

Table 6 presents a comprehensive statistical evaluation of the algorithms' performance in minimizing active power losses. This detailed analysis provides deeper insights into the reliability, consistency, and overall effectiveness of each algorithm across multiple runs. The standard deviation (STD) values offer crucial information about the algorithms' stability. AHA demonstrates the highest stability with an exceptionally low standard deviation of 0.00857, suggesting highly consistent performance across runs. Conversely, AOA shows the highest variability with a standard deviation of 1.58260, indicating less predictable performance. The percentage relative error (%RE) further corroborates these findings. AHA exhibits the lowest %RE at 0.00112%, while AOA has the highest at 2.84340%. This substantial difference underscores AHA's superior consistency in finding near-optimal solutions. Mean Absolute Error (MAE) and Mean Squared Error (MSE) provide additional measures of algorithm accuracy. AHA again outperforms other algorithms with the lowest MAE (0.000934) and MSE (7.4185e−05), while AOA shows the highest values (MAE: 2.44640, MSE: 8.484700), indicating larger deviations from the optimal solution. The Root Mean Square Logarithmic Error (RMSLE) values, which are less sensitive to outliers, show a similar trend. AHA has the lowest RMSLE (4.4194e−05), while AOA has the highest (0.0145780), further confirming AHA's superior performance and consistency. Median and mode values provide insights into the central tendency of the solutions. For most algorithms, including AHA, BES, EO, and INFO, the median and mode are close to or equal to the global optimum (83.593 kW), indicating that these algorithms frequently achieve near-optimal solutions. The variance, which measures the spread of solutions, is lowest for AHA (7.344e−05) and highest for AOA (2.5047), once again highlighting the stark contrast in consistency between these two algorithms.

Table 6: Statistical performance metrics of metaheuristic algorithms for power loss minimization

Algorithms name	STD (σ)	SE	%RE	MAE	MSE	RMSLE	Median	Mode	Variance
AHA	0.00857	0.0003556	0.00112	0.000934	7.4185e−05	4.4194e−05	83.593	83.593	7.344e−05
AOA	1.58260	0.0707780	2.84340	2.44640	8.484700	0.0145780	85.676	84.899	2.5047
BES	0.13650	0.0061045	0.22618	0.18950	0.054504	0.0011958	83.730	83.73	0.018632
DE [26]	0.18396	0.0082269	0.36371	0.30515	0.126890	0.0018235	83.772	83.731	0.033841
EO [26]	0.14684	0.0065734	0.21674	0.18158	0.054490	0.0011956	83.730	83.730	0.021562
FDA	0.26245	0.0117370	0.28279	0.23706	0.124940	0.0018044	83.731	83.731	0.068881
GBO	0.12101	0.0054115	0.14478	0.12120	0.029302	0.0008770	83.730	83.593	0.014642
GNDO	0.64424	0.0288110	1.52170	1.29170	2.082600	0.0073259	84.781	84.438	0.41505
INFO	0.07488	0.0033487	0.09018	0.07545	0.011289	0.0005450	83.730	83.593	0.005607
MPA	0.16046	0.0071759	0.19035	0.15943	0.051112	0.0011577	83.731	83.731	0.025747
RKO	0.17522	0.0078362	0.12820	0.10731	0.042156	0.0010507	83.593	83.593	0.030703
SMA [26]	0.28441	0.0127190	0.18425	0.15430	0.104530	0.0016445	83.730	83.730	0.080886

5.1.4 Computational Efficiency Analysis

Table 7 provides crucial information about the computational efficiency of each algorithm by comparing their elapsed times in solving the reconfiguration problem. AOA demonstrates the highest efficiency with an average elapsed time of 28.322 s, significantly lower than other algorithms. This suggests that AOA, despite its lower accuracy in finding optimal solutions, excels in computational speed. On the other end of the spectrum, GNDO requires the most time with an average of 1668.014 s. This extended computation time could be a significant drawback in real-time or large-scale applications, despite the algorithm's performance regarding solution quality. It's noteworthy that some algorithms, such as DE and SMA, strike a balance between solution quality and computational efficiency. DE, for instance, has a relatively low average elapsed

time of 193.8 s while maintaining good performance in solution quality as seen in Table 6. The range of elapsed times, indicated by the maximum and minimum times, varies significantly among algorithms. FDA shows the widest range (415.6537 to 1395.7252 s), while DE demonstrates the narrowest range (175.3946 to 211.7407 s), suggesting more predictable runtime for DE. The presence of outliers, as indicated in the last column, suggests that some algorithms (particularly AHA and BES) occasionally require significantly more time than their typical performance, which could be a consideration in time-sensitive applications.

Table 7: Computational efficiency: elapsed time analysis of metaheuristic algorithms in network reconfiguration

Algorithms name	Duration time (Seconds)						
	Maximum time	Minimum time	Average time	Median time	Upper adjacent	Lower adjacent	Outliers no.
AHA	611.72	354.62	432.95	424.03	544.1632	354.6162	11
AOA	56.209	10.3374	28.322	28.663	47.7984	10.3374	5
BES	589.3029	318.8621	384.76	381.92	437.0547	330.0483	18
DE [33]	211.7407	175.3946	193.8	193.69	211.7407	175.3946	0
EO [33]	691.8054	179.9317	339.14	307.33	595.6451	179.9317	10
FDA	1395.7252	415.6537	864.776	854.36	1326.2993	415.6537	1
GBO	701.7509	105.0298	324.86	302.55	701.7509	105.0298	0
GNDO	1800.9776	1536.5977	1668.014	1669.34	1775.5735	1561.3288	4
INFO	907.8062	345.5782	622.5717	616.2508	907.8062	345.5782	0
MPA	1498.2366	842.3177	1225.4	1232.4329	1498.2	842.32	0
RKO	1494.7617	466.1975	1072.9	1083.2	1494.7617	543.7039	1
SMA [33]	559.8522	94.2545	254.54	226.16	506.4191	94.2545	3

The statistical evaluation and elapsed time analysis provide a more nuanced understanding of the algorithms' performance. While AHA excels in finding high-quality solutions consistently, it comes at the cost of higher computational time. AOA, on the other hand, offers rapid computation but with less consistent and often suboptimal solutions. Algorithms like INFO and GBO emerge as strong candidates for this particular problem, providing a good balance with respect to solution quality, consistency, and computational efficiency. However, the specific requirements of the application, such as real-time constraints or the need for extremely stable performance, may favor different algorithms in certain scenarios. These findings underscore the importance of comprehensive performance evaluation in metaheuristic optimization, going beyond just the quality of the best solution found. Future research could explore hybrid approaches that combine the strengths of multiple algorithms to achieve even better overall performance in power distribution system optimization.

5.1.5 Visual Performance Analysis

To provide a more intuitive understanding of the algorithms' performance, visual representations of key metrics are presented. Fig. 6 illustrates the distribution of elapsed time for each algorithm across 500 runs.

The box plot in Fig. 6 provides a clear visualization of the computational efficiency across all twelve algorithms. Each box represents the distribution of elapsed time (in seconds) over 500 independent runs, with the central line indicating the median time, while the box edges mark the first and third quartiles. This visualization reveals significant variations in computational requirements, with AOA demonstrating the fastest average execution time (28.32 s), though its other performance metrics are suboptimal. Conversely,

algorithms like GNDO and MPA exhibit substantially longer computation times (1668.01 and 1225.4 s, respectively), which may limit their practical applicability despite reasonable optimization capabilities. The AHA algorithm shows moderate computational requirements (432.95 s) while maintaining superior performance in other critical metrics. This time performance analysis is essential for real-world implementation considerations, where computational resources may be constrained or where reconfiguration decisions must be made within specific time windows.

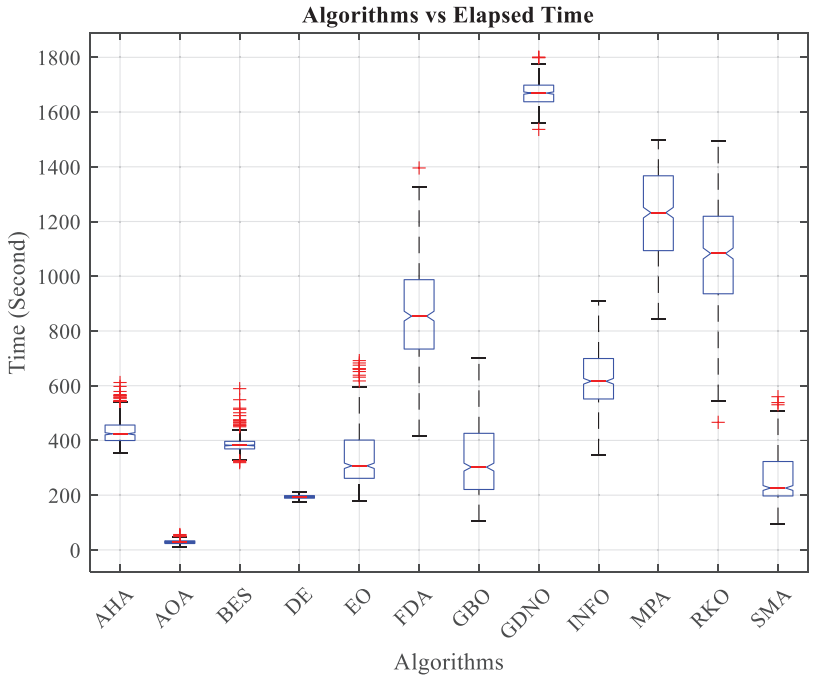

Figure 6: Algorithms performance vs. time elapsed

Fig. 7 presents a radar chart comparing critical performance metrics of the most effective algorithms for unbalanced power distribution network reconfiguration.

The radar chart (Fig. 7) clearly illustrates the exceptional performance of the AHA algorithm across critical metrics for UPDN reconfiguration. AHA demonstrates overwhelming superiority in four of the five key performance indicators: achieving near-perfect global optimum detection (493/500 runs), exhibiting remarkable consistency with the lowest standard deviation (0.008), delivering the highest power loss reduction even in worst-case scenarios (12.4%), and maintaining minimal error rates (MAE = 0.0009). While SMA shows better computational speed, AHA's commanding lead in these more critical metrics establishes it as the most effective algorithm for unbalanced power distribution network reconfiguration. This balanced excellence across multiple performance dimensions confirms AHA's robustness and reliability for practical UPDN applications, making it the clear choice for network operators and system designers.

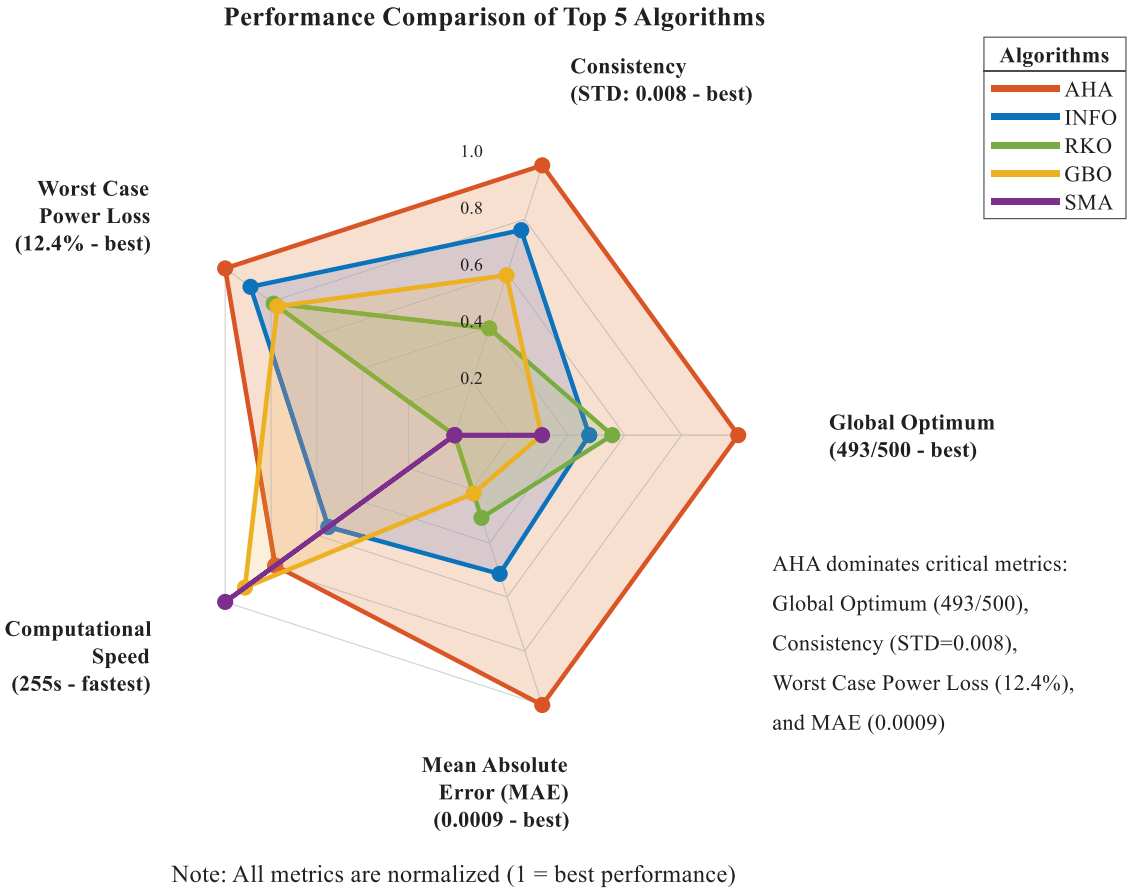

Figure 7: Critical performance metrics comparison of metaheuristic algorithms for UPDN reconfiguration

5.1.6 Summary of Scenario I Findings

This comprehensive analysis of twelve metaheuristic optimization algorithms for minimizing active power losses in the IEEE 123-Bus test system reveals significant variations in performance, consistency, and convergence characteristics. While several algorithms demonstrated the ability to achieve the global optimum, their reliability and computational efficiency differed substantially. The analysis of worst-case scenarios and average power losses further highlights the trade-offs between achieving optimal solutions and maintaining consistent performance across multiple runs.

The statistical evaluation and elapsed time analysis provide a more nuanced understanding of the algorithms' performance. While AHA excels in finding high-quality solutions consistently, it comes at the cost of higher computational time. AOA, on the other hand, offers rapid computation but with less consistent and often suboptimal solutions. Algorithms like INFO and GBO emerge as strong candidates for this particular problem, offering a good balance between solution quality, consistency, and computational efficiency.

The visual representations in Figs. 6 and 7 complement the quantitative analyses and provide an intuitive understanding of the relative performance differences between algorithms. These findings provide valuable insights for selecting appropriate algorithms for similar power system optimization problems and highlight areas for potential algorithmic improvements. Future research could explore hybrid approaches that combine the strengths of multiple algorithms to achieve even better overall performance in power distribution system optimization.

5.2 Scenario II: Power Quality Improvement

The purpose of scenario II is to minimize the unbalanced indices by treating them as a fitness function. The unbalance index formula is detailed in Eq. (11). In this part, the data and conditions from the first scenario are utilized to ensure the reproducibility of the analysis and to elevate the level of calculation complexity. Various cases are examined to reduce the VUI and CUI within the 123-Bus UPDN.

- In the first situation, the reconfiguration process is employed to minimize the average values of the CUI and VUI across the whole system (Case-1)
- In the subsequent case, the objective is to reduce the maximum recorded values of the VUI and CUI (Case-2)
- In the third instance, the focus is on minimizing the CUI measurement at the feeder point (Case-3)

The VUI is capped at 3%, and while there is no formal standard for the CUI, the recommended threshold is 30% [33]. Additionally, while the specified 30% limit for CUI is met in small-scale test systems, it exceeds this threshold in larger-scale power systems. The CUI estimation technique has proven effective for smaller-scale test systems, particularly those with 25-bus and 19-bus unbalanced setups, as highlighted in Ref. [32]. However, its effectiveness decreases when used for larger systems, like the 123-Bus UPDN, where it does not yield solutions recognized as acceptable by current standards. For example, in the initial setup, the peak value of the CUI at bus-65 is 45.72%, which exceeds the recommended limit of 30%. In this study, the reconfiguration approach reduced the average CUI value from 13.345% to 7.867%.

5.2.1 Current Unbalance Index Optimization in UPDN: A Comprehensive Analysis

This research investigates the optimization of PDNs through network reconfiguration techniques, focusing on the minimization of the CUI in a 123-Bus IEEE-PES test system. The study employs various objective functions to reconfigure the network, aiming to achieve optimal CUI values while considering the complex interplay between current balance, power losses, and voltage profiles. By systematically applying different optimization criteria, this work seeks to elucidate the efficacy and trade-offs associated with reconfiguration in enhancing the overall performance and stability of unbalanced distribution networks. In Table 8, five cases are analyzed, each targeting different aspects of system performance. In the IEEE-PES (123-Bus test system) solution, currents at the milli/micro-ampere level are neglected and assumed to be zero at all buses. In contrast, the OpenDSS simulation platform does not permit zero current values at any bus, regardless of their magnitude. This discrepancy arises from the differing approaches of the two platforms, with IEEE-PES disregarding insignificant current levels, while OpenDSS accounts for even the smallest values. In this study, the methodology followed by IEEE-PES is adopted as a reference [33].

Table 8: Results of the current unbalance index following reconfiguration

			Case-1	Case-2	Case-3
	Initial case	**Power loss as a fitness function**	**Mean of CUI**	**Min. of highest CUI**	**Min. of CUI at feeder bus (149)**
Tie-Switches	54–94, 151–300, Added TSs: 35–66, 83–195, 251–300	47–49, 64–65, 72–76, 76–77, 108–300	135–35, 89–91, 93–95, 60–160, 151–300	40–42, 53–54, 78–80, 54–94, 108–300	53–54, 91–93, 105–108, 51–151, 60–160

(Continued)

Table 8 (continued)

			Case-1	Case-2	Case-3
	Initial case	**Power loss as a fitness function**	**Mean of CUI**	**Min. of highest CUI**	**Min. of CUI at feeder bus (149)**
Feeder Bus CUI value (at Bus-149)	13.7661138	13.7044087	13.854873	14.0234191	12.7169682
Mean of CUI value	13.3451517	15.0528607	7.866602	9.7845134	15.4137881
Max. CUI value Bus No.	45.7187944, Bus-65	54.3108809, Bus-63	21.572768, Bus-76	16.958307, Bus-197	78.81678, Bus-28
Minimum Voltage Bus No., Phase	0.9858562, Bus-65, [A]	0.988303, Bus-63, [A]	0.9499476, Bus-51, [A]	0.9191833, Bus-56, [A]	0.9095662, Bus-104, [C]
Maximum Voltage Bus No., Phase	1.04375, Bus-149, [A], [B], [C]	1.04375, Bus-149, [A], [B], [C]	1.04375, Bus-149, [A], [B], [C]	1.04375, Bus-149, [A], [B], [C]	1.04375, Bus-149, [A], [B], [C]
Active [kW] & Reactive [kVAr] Power Loss	95.593872, j 192.464919	83.592732, j 169.16238	152.349216, j 263.958117	199.6303877, j 272.3923306	202.3504114, j 301.4664235
Bus Number of over the 30% CUI value	65 (45.72%), 86 (37.31%), 87 (31.98%), 91 (44.72%)	63 (54.311%), 66 (45.353%), 87 (34.894%), 89 (32.226%)	0	0	21 (46.613%), 23 (60.570%), 25 (68.770%), 28 (78.816%), 29 (75.360%), 30 (70.760%), 86 (34.271%), 97 (30.807%)

Initial Case

The initial case serves as a baseline, representing the network's configuration without optimization. The system exhibits a mean CUI of 13.345, with a maximum value of 45.719 observed at Bus-65. The feeder bus (Bus-149) demonstrates a CUI of 13.766, closely aligning with the system's average. Fig. 8 illustrates the distribution of non-zero CUI values across buses in this initial configuration, showcasing a relatively concentrated pattern with a few notable peaks representing buses with high current imbalance. The voltage profile ranges from 0.986 to 1.044 p.u., indicating relatively stable voltage conditions. However, the presence of four buses with CUI values exceeding 30% suggests significant localized current imbalances. The system experiences active and reactive power losses of 95.594 kW and 192.465 kVAr, respectively, indicating potential for efficiency improvements.

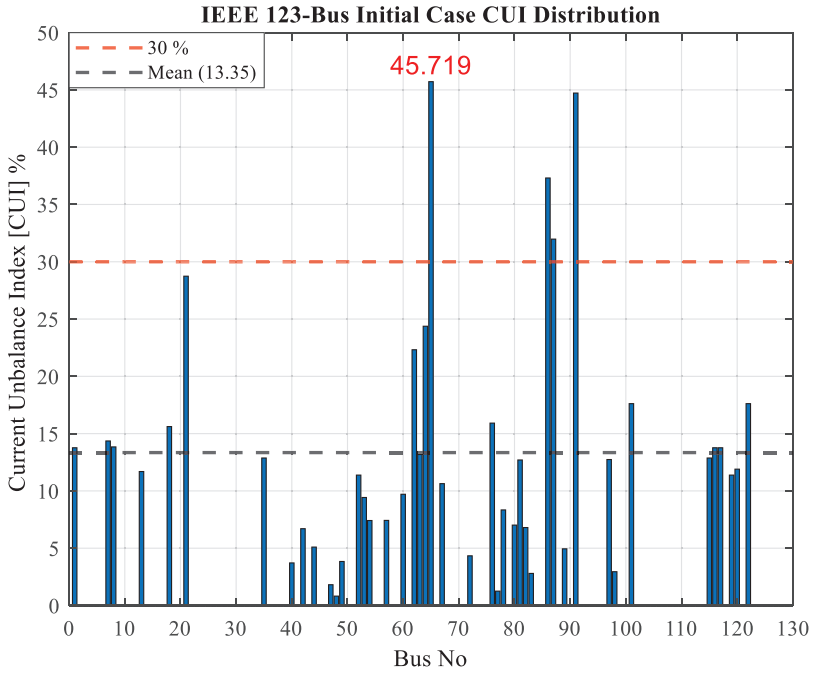

Figure 8: Distribution of non-zero CUI values across buses in the initial network configuration (initial case)

Active Power Loss Minimization

The reconfiguration strategy in this case, which prioritizes the minimization of active power losses, successfully reduces active losses to 83.593 kW, a 12.6% decrease from the initial case. Concurrently, reactive power losses decrease to 169.162 kVAr, representing a 12.1% reduction. However, this improvement in efficiency comes at the cost of slightly increased current imbalance. The mean CUI rises to 15.053, and the maximum CUI increases to 54.311 at Bus-63. Fig. 9 depicts the distribution of non-zero CUI values per bus after this reconfiguration, revealing a more pronounced spread of CUI values with higher peaks compared to the initial case. Notably, while both cases (initial and minimum active power loss case) have four buses with CUI values over 30%, their distribution changes. In this case, these buses are: Bus-63 (54.31%), Bus-66 (45.35%), Bus-87 (34.89%), and Bus-89 (32.23%). This represents a shift in the location and intensity of high CUI values compared to the initial case, which is clearly visible when comparing Figs. 8 and 9. Despite the trade-offs in current balance, the voltage profile in this case demonstrates marginal enhancement, with the minimum voltage rising to 0.988303 p.u. at Bus-63, relative to the initial case's minimum of 0.9858562 p.u. The visual comparison provided by Figs. 8 and 9 aligns with the numerical findings, clearly depicting the increased mean and maximum CUI values in the minimum active power loss configuration. This graphical representation underscores the impact of the reconfiguration strategy on current imbalance throughout the system.

In conclusion, while the active power loss minimization strategy achieves significant reductions in both reactive and active power losses, it does so at the expense of slightly increased current imbalance across the system, as evidenced by both numerical data and visual representations in Figs. 8 and 9. This trade-off highlights the complex interplay between different optimization objectives in power distribution systems and underscores the importance of multi-objective approaches in finding balanced solutions.

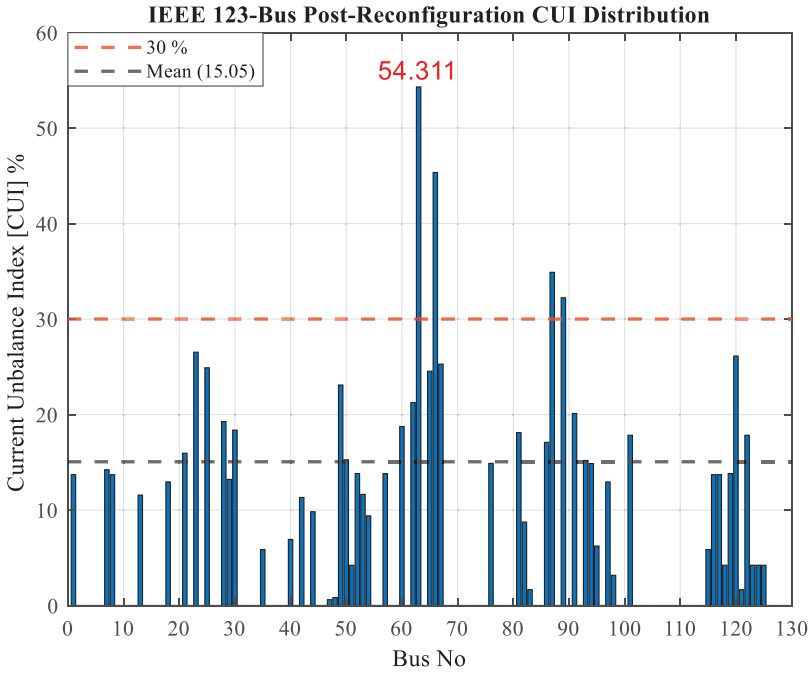

Figure 9: Non-zero CUI values per bus post-reconfiguration for active power loss minimization

Case-1: Mean CUI Optimization

Case-1 focuses on minimizing the average CUI across the entire network. This strategy proves highly effective in improving current balance, dramatically reducing the mean CUI to 7.867, a 41% improvement from the initial case. The maximum CUI also decreases significantly to 21.573 at Bus-76 as shown in Fig. 10, and notably, no buses exhibit CUI values exceeding 30%. However, this substantial improvement in current balance comes at a considerable cost to system efficiency. Active power losses increase dramatically to 152.349 kW, representing a 59.4% increase from the initial case. This stark contrast highlights the severe conflict between CUI optimization and power loss minimization. Additionally, the voltage profile slightly deteriorates, with the minimum voltage dropping to 0.950 p.u. at Bus-51 as shown in Fig. 11.

Case-2: Peak CUI Optimization

The third reconfiguration strategy (Case-2) aims to reduce the peak CUI values in the system. This approach successfully lowers the maximum CUI to 16.958 at Bus-197 as shown in Fig. 12, a substantial 62.9% reduction from the initial case. The mean CUI also improves to 9.785, indicating a generally more balanced system. However, the focus on minimizing the highest CUI values leads to a substantial increase in active power losses, peaking at 199.630 kW—an astonishing 108.8% rise compared to the initial case. This scenario also causes a noticeable deterioration in the voltage profile, with the minimum voltage dropping to 0.919 p.u. at Bus-56 as shown in Fig. 13, marking the most significant impact on voltage regulation among all the cases analyzed.

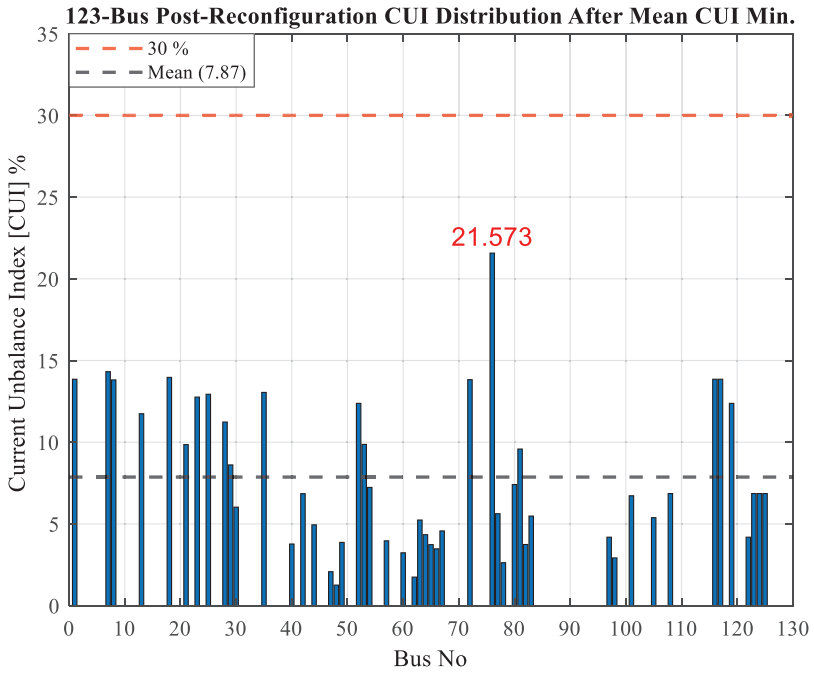

Figure 10: Bus-wise non-zero CUI values following reconfiguration aimed at minimizing mean CUI

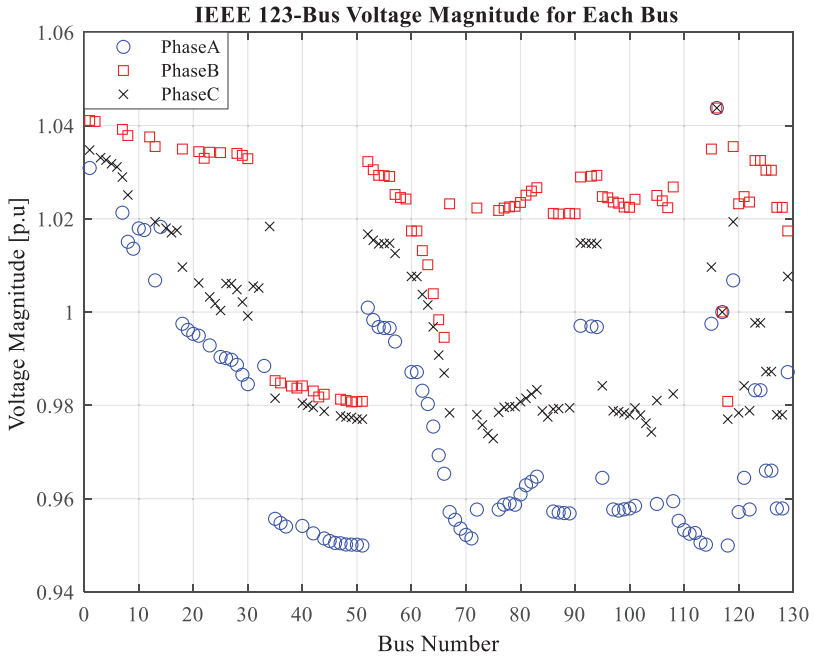

Figure 11: Voltage profile for mean CUI minimization in the 123-Bus UPDN

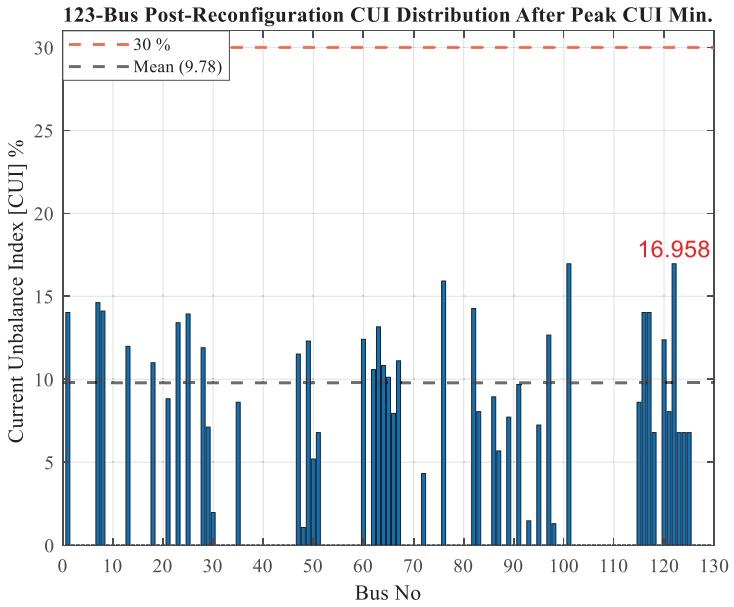

Figure 12: Distribution of non-zero CUI values across buses after reconfiguration to minimize the highest CUI value

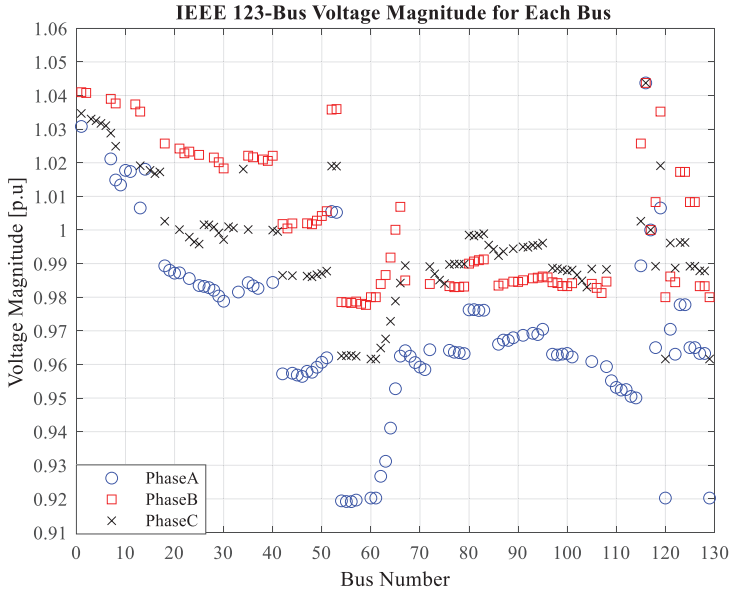

Figure 13: Voltage profile for peak CUI minimization in the 123-Bus UPDN

Case-3: CUI Minimization at the Feeder Bus

The final reconfiguration strategy (Case-3) targets CUI minimization specifically at the feeder bus (Bus-149). This approach effectively reduces the feeder bus CUI to 12.717, the lowest among all cases. However, this localized optimization leads to unintended consequences elsewhere in the network. The mean CUI increases to 15.414, higher than in Cases 1 and 2, indicating that focusing on a single point may worsen overall system balance. Moreover, this case results in the highest maximum CUI (78.817 at Bus-28 as shown

in Fig. 14) and the most buses (8) with CUI values over 30%, suggesting significant imbalances in parts of the network. The voltage profile in this scenario is the poorest among all cases, with the minimum voltage dropping to 0.910 p.u. at Bus-104, as shown in Fig. 15. Active power losses increase substantially to 202.350 kW, a 111.7% rise from the initial case, further emphasizing the trade-off between localized CUI improvement and system-wide efficiency.

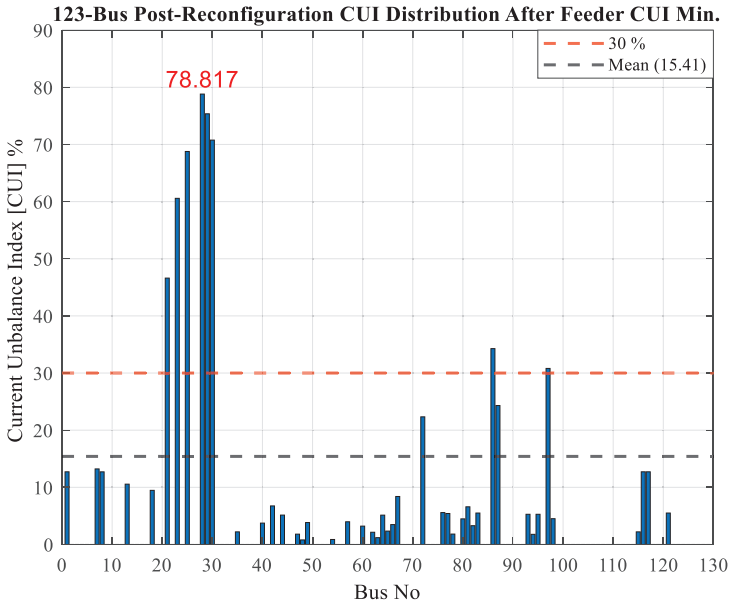

Figure 14: Non-zero CUI values per bus after reconfiguration, focusing on CUI minimization at the feeder bus (Case-3)

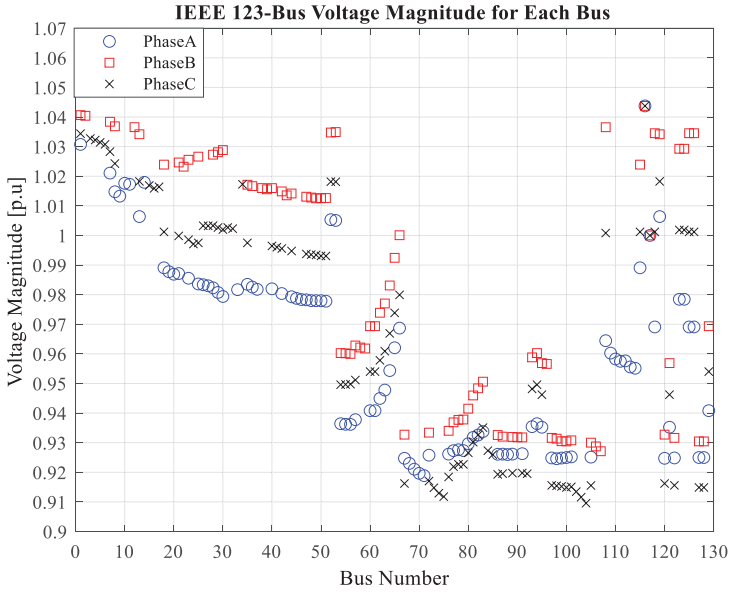

Figure 15: Voltage profile for feeder-bus CUI minimization in the 123-Bus UPDN

5.2.2 Voltage Unbalance Index Optimization in UPDN: A Comprehensive Analysis

This research explores the application of network reconfiguration techniques to optimize power distribution systems, with a primary focus on minimizing the VUI. The study employs network reconfiguration techniques to minimize voltage unbalance, considering various objective functions and constraints. The section focuses on two primary cases:

- Case-1 aims to minimize the mean VUI values across the entire system through reconfiguration.
- Case-2 focuses on reducing the maximum VUI values in the network.

Both cases utilize network reconfiguration strategies to achieve their respective objectives while maintaining system constraints such as radial topology, voltage limits, and power flow requirements. This approach not only targets the enhancement of voltage balance but also provides significant insights into the intertwined nature of multiple system parameters within the context of distribution network optimization. The study compares these optimization approaches against the initial case and a power loss minimization case to analyze the effectiveness of different strategies in enhancing voltage balance within the distribution network.

Initial Case

The initial case, as depicted in Fig. 16 and detailed in Table 9, serves as the baseline for the analysis. Fig. 16 illustrates the voltage profile for the initial case in the 123-Bus UPDN, providing a visual representation of voltage variations across the system. Complementing this, Fig. 17 showcases the distribution of the VUI values, offering insights into the spatial patterns of voltage imbalances throughout the network. In this configuration, the system exhibits a mean VUI of 0.867, with maximum VUI values of 1.0781 observed at Bus-95 and Bus-195. Notably, 19 buses demonstrate VUI values exceeding 1%, which surpasses the stringent limit set by the NEMA. This initial state, as evidenced by both the voltage profile and VUI distribution, indicates significant voltage imbalances across the network, warranting optimization efforts to improve overall system performance and power quality.

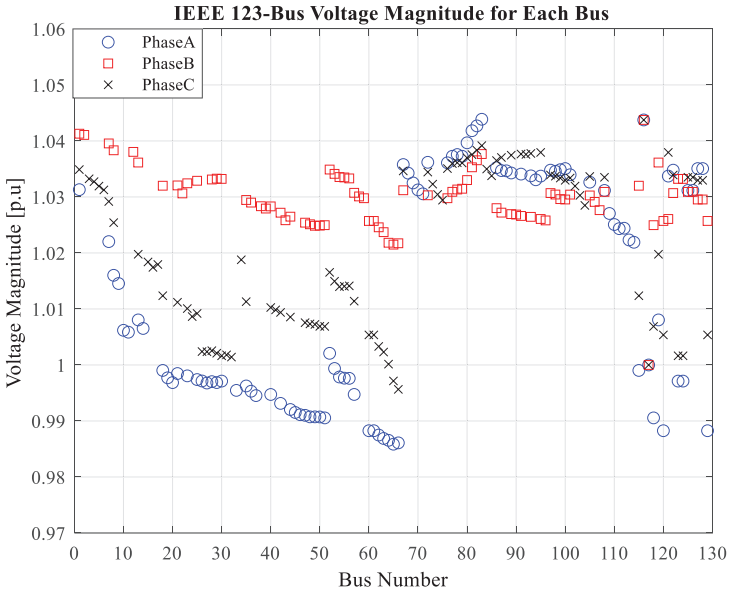

Figure 16: Voltage profile for the initial case in 123-Bus UPDN

Table 9: Comparative analysis of VUI optimization scenarios in the 123-Bus UPDN

			Case-1	Case-2
	Initial case	**Power loss as a fitness function**	**Mean value of VUI**	**Minimum of the maximum VUI value**
Tie-switches	54–94, 151–300, Added TSs: 35–66, 83–195, 251–300	47–49, 64–65, 72–76, 76–77, 108–300	44–47, 57–60, 81–82, 91–93, 101–105	44–47, 54–57, 89–91, 93–95, 101–105
VUI value at feeder bus (at Bus 149)	1.5857e−14	1.5857e−14	1.5857e−14	1.5857e−14
Mean of VUI value	0.867437048	0.81577365	0.6178654	0.7173793
Maximum VUI value bus no.	1.0780543644, Bus-95, and Bus-195	1.0565566, Bus-63	1.138647, Bus-60, and Bus-160	0.8446299, Bus-48
Minimum voltage bus no., Phase	0.9858562, Bus-65, [A]	0.9883316, Bus-63, [A]	0.9393997, Bus-60, [C]	0.9424907, Bus-114, [A]
Maximum voltage bus no., Phase	1.04375, Bus-149, [A], [B], [C]	1.04375, Bus-149, [A], [B], [C]	1.048999, Bus-82, [B]	1.04375, Bus-149, [A], [B], [C]
Active [kW] & Reactive [kVAr] Power loss	95.593872, j192.464919	83.5927322, j 169.0420380	167.5974679, j 252.7814353	161.3500279, j 244.5218031
Bus numbers with VUI values exceeding 1%	60, 61, 62, 63, 64, 65, 86, 87, 89, 91, 93, 95, 105, 108, 160, 195, 300, 350, 610	60, 61, 62, 63, 64, 160, 610,	60, 61, 62, 63, 160, 610	0

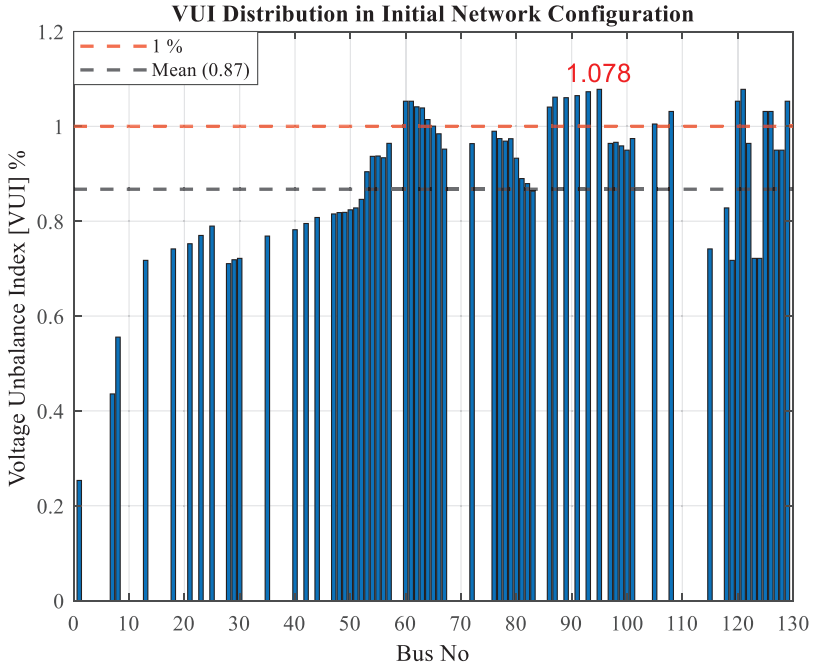

Figure 17: Distribution of VUI in the initial 123-Bus UPDN configuration

Minimum Power Loss Case

The scenario prioritizing active power loss reduction, as depicted in Fig. 18 (voltage profile) and Fig. 19 (VUI distribution), demonstrates the effects of network reconfiguration aimed at reducing active power losses. Table 9 presents a detailed comparative analysis of the initial case and this optimized scenario. The reconfiguration process successfully decreases active power losses from 95.593 to 83.593 kW, representing a significant 12.56% reduction. Concurrently, reactive power losses diminish from 192.465 to 169.042 kVAr. This substantial improvement in power efficiency is achieved through strategic changes in the network

topology, as evidenced by the altered tie-switch positions (47–49, 64–65, 72–76, 76–77, 108–300). The impact of this loss-focused reconfiguration on voltage balance presents a nuanced picture. The mean VUI shows a modest enhancement, reducing from 0.867 to 0.816. The maximum VUI experiences a slight decrease from 1.079 (initially at Bus-95 and Bus-195) to 1.057 at Bus-63. This shift in the location and magnitude of maximum VUI, which is clearly visible in Fig. 19, indicates a redistribution of voltage imbalances across the network as a consequence of the loss minimization strategy.

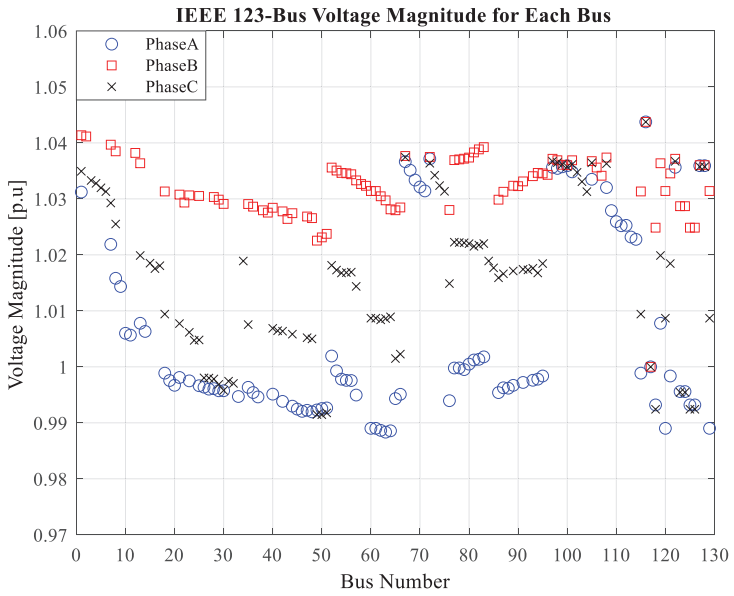

Figure 18: Voltage profile for the minimum power loss in 123-Bus UPDN

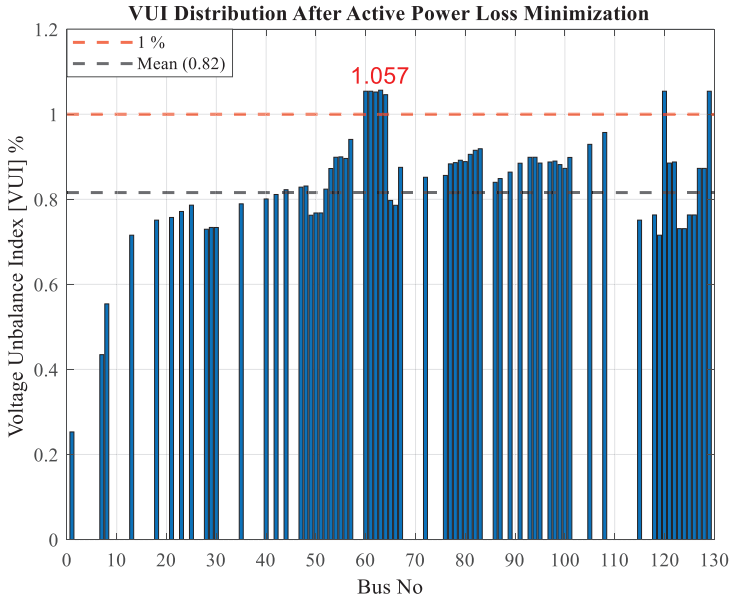

Figure 19: Distribution of VUI in the minimum active power loss configuration

The voltage profile, illustrated in Fig. 18, reveals a marginal enhancement in the overall voltage conditions. The minimum voltage rises slightly from 0.986 to 0.988 p.u., both occurring at phase A, but shifting from Bus-65 to Bus-63. The maximum voltage remains constant at 1.044 p.u. at Bus-149 across all phases, suggesting that the upper voltage limit is unaffected by the reconfiguration process. Notably, the number of buses experiencing VUI values greater than 1% reduces from 19 in the initial case to 7 in the optimized scenario. This significant reduction, prominently displayed in the VUI distribution of Fig. 19, signifies an overall enhancement of voltage balance throughout the network, despite the slight increase in maximum VUI. These results underscore the complex interplay between power loss reduction and voltage balance in distribution networks. While the reconfiguration effectively reduces system losses, its impact on voltage unbalance is mixed. This outcome suggests that while prioritizing active power loss reduction can yield substantial efficiency gains, a multi-objective optimization approach might be necessary to achieve comprehensive improvements in both power efficiency and voltage quality simultaneously.

Case-1: Mean VUI Optimization

Case-1 optimizing the mean VUI, as illustrated in Fig. 20 (voltage profile) and Fig. 21 (VUI distribution), demonstrates the effects of network reconfiguration aimed at improving voltage balance across the system. The reconfiguration process targeting mean VUI minimization yields significant improvements in voltage balance. The mean VUI experiences a substantial reduction from the initial 0.8674 to 0.6178, representing a 28.8% improvement. This marked enhancement in voltage balance is visually evident in the VUI distribution depicted in Fig. 21, showing a more uniform and lower range of VUI values across the network. However, this improvement in overall voltage balance comes with a trade-off in terms of maximum VUI. The maximum VUI increases from 1.0781 (initially at Bus-95 and Bus-195) to 1.139 at Bus-60 and Bus-160. This shift, while increasing the peak VUI, is combined with a significant decrease in the number of buses experiencing VUI values greater than 1%, decreasing from 19 in the initial case to only 6 in the optimized scenario. The voltage profile, as shown in Fig. 20, indicates some changes in the network's voltage characteristics. The minimum voltage decreases slightly from 0.986 p.u. (Bus-65, Phase A) to 0.939 p.u. (Bus-60, Phase C), while the maximum voltage reaches 1.048999 p.u. at Bus-82, Phase B.

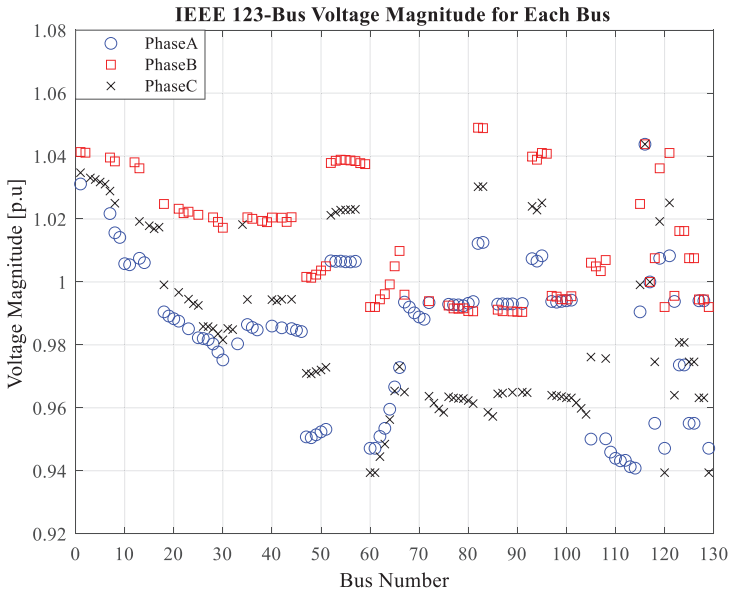

Figure 20: Voltage profile for mean VUI minimization in the 123-Bus UPDN

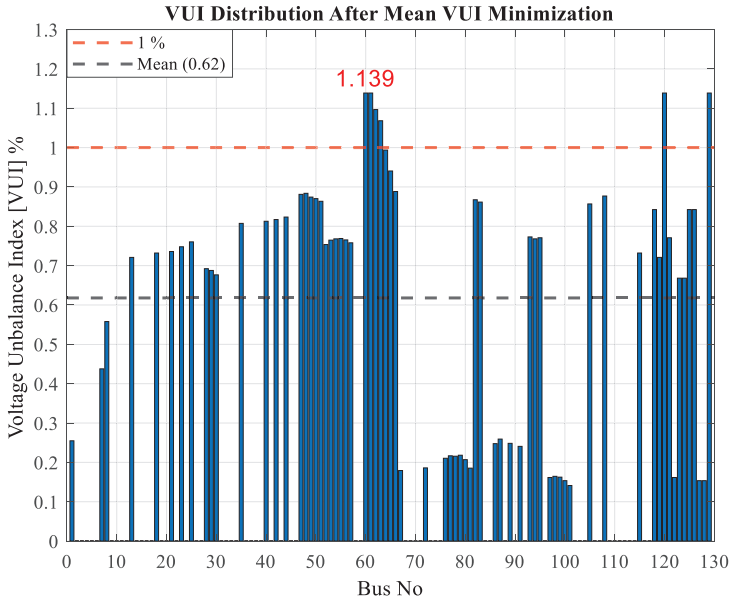

Figure 21: Distribution of VUI in the mean VUI minimization configuration

Interestingly, the focus on voltage balance leads to a significant increase in active power losses, from 95.594 kW in the initial case to 167.597 kW in the optimized scenario. This 75.3% increase in active power losses demonstrates the complex relationship between current balance and system efficiency. While improving current balance significantly enhances voltage quality across the network, it comes at the cost of increased power losses. The reactive power losses also see a substantial increase from 192.465 to 252.7814 kVAr, further emphasizing the trade-off between current balance and power efficiency.

This outcome underscores the intricate interplay between voltage balance and power losses in distribution networks. While the mean VUI optimization successfully improves overall voltage balance and reduces the prevalence of high VUI values, it does so at the expense of increased power losses and a slightly higher maximum VUI. The results suggest that while focusing on voltage balance can lead to significant improvements in voltage quality across the network, it may not be the most effective strategy for minimizing power losses. This demonstrates the role of multi-objective optimization strategies that can balance the competing goals of improving voltage quality and maintaining system efficiency.

Case-2: Peak VUI Optimization

The scenario optimizing the peak VUI, as illustrated in Fig. 22 (voltage profile) and Fig. 23 (VUI distribution), demonstrates the effects of network reconfiguration aimed at minimizing the highest VUI value in the UPDN. Table 9 provides a comprehensive evaluation of differences between the initial case and this optimized scenario (Case-2). The reconfiguration process targeting peak VUI minimization yields significant improvements in voltage balance across the network. The maximum VUI value experiences a notable decline from the initial 1.078 (at Bus-95 and Bus-195) to 0.845 (at Bus-48), representing a 21.7% improvement. This marked enhancement in peak voltage balance is visually evident in the VUI distribution depicted in Fig. 23, showing a more compressed range of VUI values across the network. While the optimization focuses on minimizing the peak VUI, it also results in an improvement in the mean VUI, which decreases from 0.867 to 0.717, a 17.3% reduction. The voltage profile, as shown in Fig. 22, indicates some changes in the network's voltage characteristics. The minimum voltage actually decreases slightly from 0.986 p.u. (Bus-65, Phase A) in the initial case to 0.942 p.u. (Bus-114, Phase A) in the optimized scenario.

This observation shows that the optimization for minimizing the highest VUI value resulted in a slight reduction in the minimum voltage, not an improvement as previously stated. The voltage has decreased by about 0.0434 p.u., or approximately 4.34%. A remarkable outcome of this optimization is the complete elimination of buses with VUI values exceeding 1%.

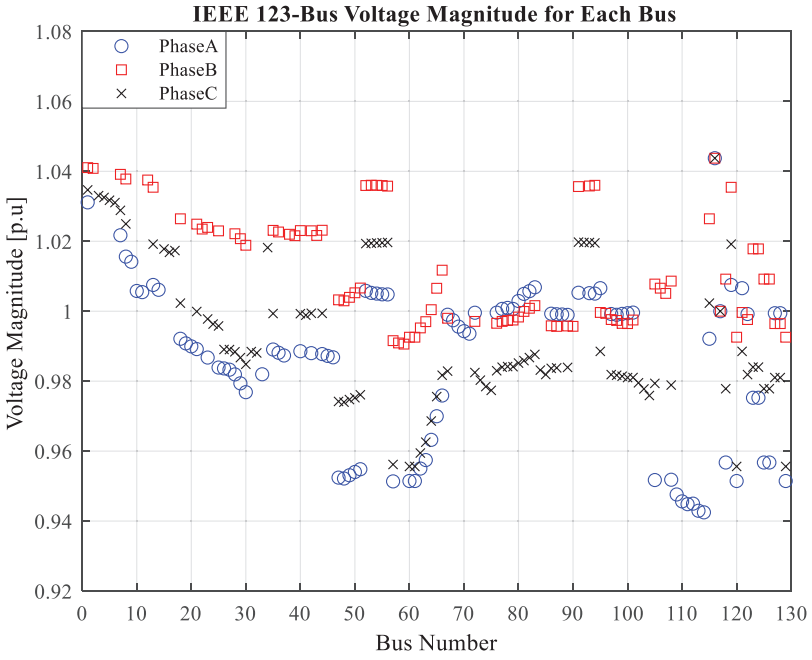

Figure 22: Voltage profile for peak VUI minimization in the 123-Bus UPDN

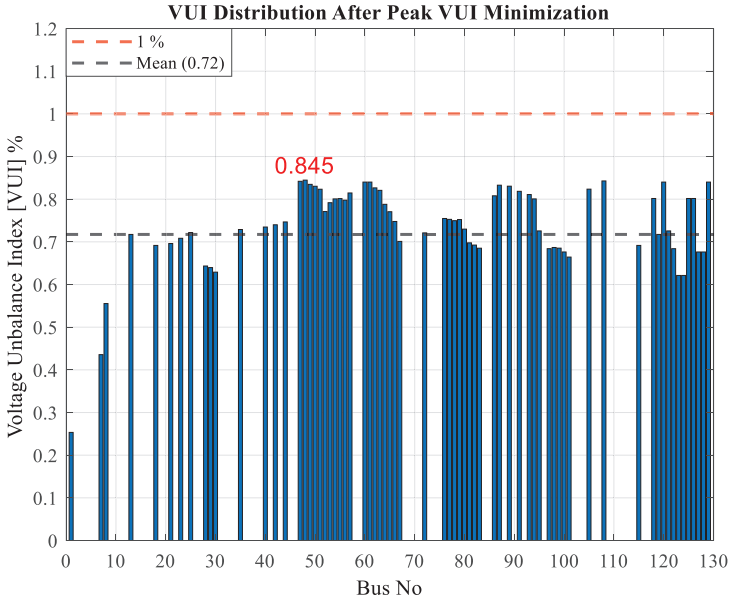

Figure 23: Distribution of VUI in the peak VUI minimization configuration

In the initial case, 19 buses had VUI values above this threshold, while in the optimized scenario, this number is reduced to zero. This significant improvement in voltage balance is clearly visible in the VUI distribution shown in Fig. 23. However, the focus on minimizing peak VUI comes with a trade-off in terms of power losses. The active power losses increase from 95.593 kW in the initial case to 161.350 kW in the optimized scenario, representing a 68.8% increase. Similarly, reactive power losses rise from 192.465 to 244.522 kVAr. This outcome underscores the complex relationship between power losses and voltage balance in PDNs. While the peak VUI optimization successfully improves overall voltage balance and eliminates high VUI values, it results in increased power losses. The results suggest that while focusing on minimizing peak VUI can lead to significant improvements in voltage quality across the network, particularly in reducing extreme voltage imbalances, it may not be the most effective strategy for minimizing power losses. This highlights the need for multi-objective optimization strategies that can balance the competing goals of improving voltage quality and maintaining system efficiency.

The choice of optimization strategy significantly impacts tie-switch configurations, voltage profiles, and the distribution of voltage imbalances across the network. Case-2 stands out for its ability to eliminate all instances of VUI exceeding 1%, fully complying with NEMA standards, but at the cost of substantial efficiency losses. This study underscores the need for a nuanced approach to distribution network reconfiguration when addressing voltage imbalances. While all reconfiguration strategies improve upon the initial case in terms of VUI metrics, they do so with varying degrees of success and with different trade-offs in system efficiency and voltage profiles. The findings suggest that network operators must carefully weigh the benefits of improved voltage balance against the costs of increased power losses. In scenarios where voltage imbalance is causing significant issues, such as equipment malfunction or reduced system reliability, the increased losses associated with VUI minimization strategies might be justified.

5.3 Scenario III: Multi-Objective Optimization for Power Distribution System Reconfiguration

In this scenario, a multi-objective optimization approach is employed to address the complex challenges inherent in power distribution system reconfiguration. This comprehensive strategy aims to simultaneously optimize three strategic components influencing system performance: voltage unbalance, active power loss, and current unbalance. By considering these multiple objectives concurrently, this study seeks to provide a more holistic solution to the reconfiguration problem, balancing the often-competing demands of system efficiency and stability.

The multi-objective optimization problem is formulated with three distinct objective functions:

- Minimization of Active Power Loss (Ploss): This objective focuses on reducing the overall system losses, thereby enhancing the efficiency of power distribution. Reducing the power loss not only enhances system performance but also contributes to economic and environmental benefits by reducing wasted energy.
- Minimization of Mean VUI: The Mean VUI represents the average voltage imbalance across the entire system. By minimizing this value, the optimization aims to enhance the overall voltage stability and quality throughout the network, ensuring a more uniform and balanced voltage profile. This approach targets the reduction of voltage imbalances on a system-wide scale, potentially enhancing power quality, reducing equipment stress, and improving the overall reliability of the distribution network. By focusing on the mean VUI, the optimization strategy addresses the general health of the system rather than concentrating solely on localized extreme cases, thus promoting a more holistic improvement in voltage balance across all nodes of the network.

- Minimization of Mean CUI: This objective targets the average current imbalance throughout the system. Minimizing the mean CUI helps in achieving a more balanced load distribution, potentially reducing stress on system components and improving overall reliability.

The multi-objective optimization yielded a rich set of Pareto-optimal solutions, visualized through both two-dimensional and three-dimensional Pareto fronts. These visualizations provide profound insights into the intricate balance between competing system priorities.

Fig. 24 illustrates the Pareto front between Active Power Loss and Mean CUI, demonstrating the inverse relationship between system efficiency and current balance. As power losses decrease, there is a tendency for current imbalance to increase, highlighting the challenge of simultaneously optimizing both parameters.

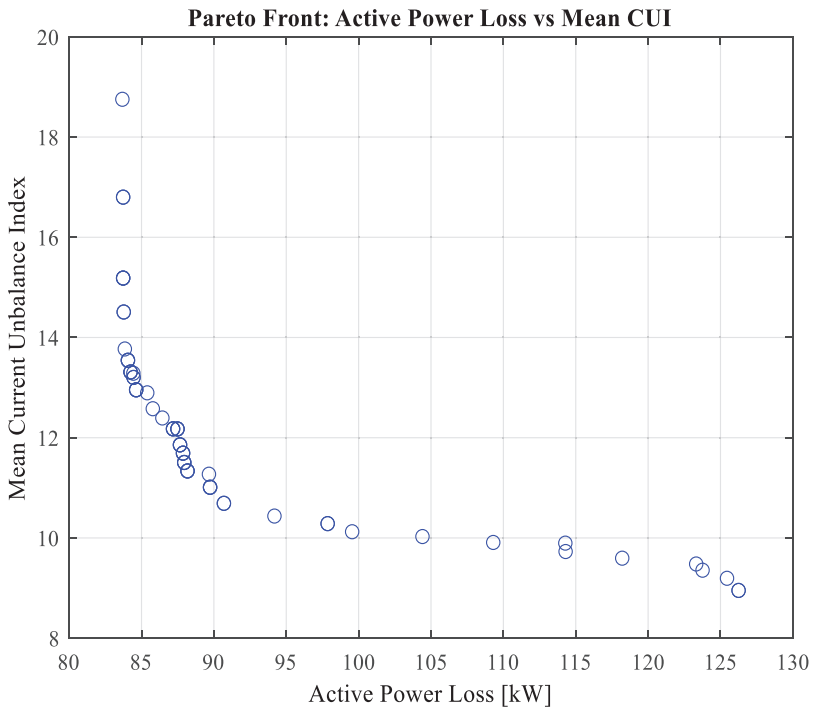

Figure 24: 2-D Pareto front illustrating the trade-off between active power loss and mean CUI

Fig. 25 presents the Pareto-optimal solutions for Active Power Loss versus Mean VUI. This relationship reveals how efforts to minimize power losses can impact voltage stability across the network. The non-linear nature of this Pareto front suggests that significant improvements in one parameter may come at the cost of marginal degradations in the other, particularly at the extremes of the optimization spectrum.

Fig. 26 depicts the trade-off between Mean CUI and Mean VUI, showcasing the delicate balance between current and voltage stability in the system. The shape of this curve indicates that there exists a range of solutions where both current and voltage imbalances can be minimized concurrently, albeit with diminishing returns at the extremes.

The three-dimensional Pareto surface illustrated in Fig. 27 provides a comprehensive visualization of the optimization landscape. This surface encapsulates the complex interactions among all three objectives, offering decision-makers a powerful tool for identifying solutions that balance multiple system priorities effectively. The non-linear relationships between different system parameters underscore the complexity

of power distribution networks and the potential for unintended consequences when optimizing for a single objective.

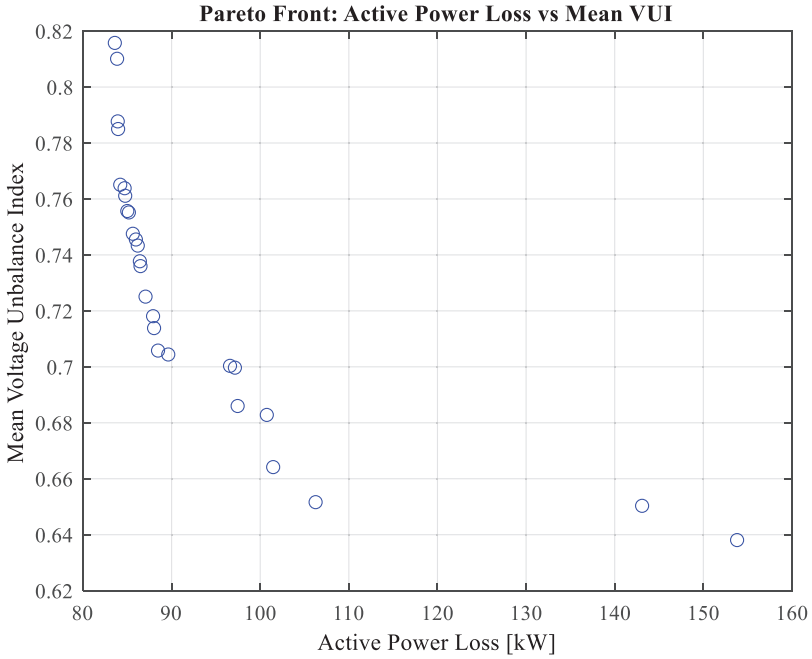

Figure 25: 2-D Pareto optimal solutions showing the relationship between active power loss and mean VUI

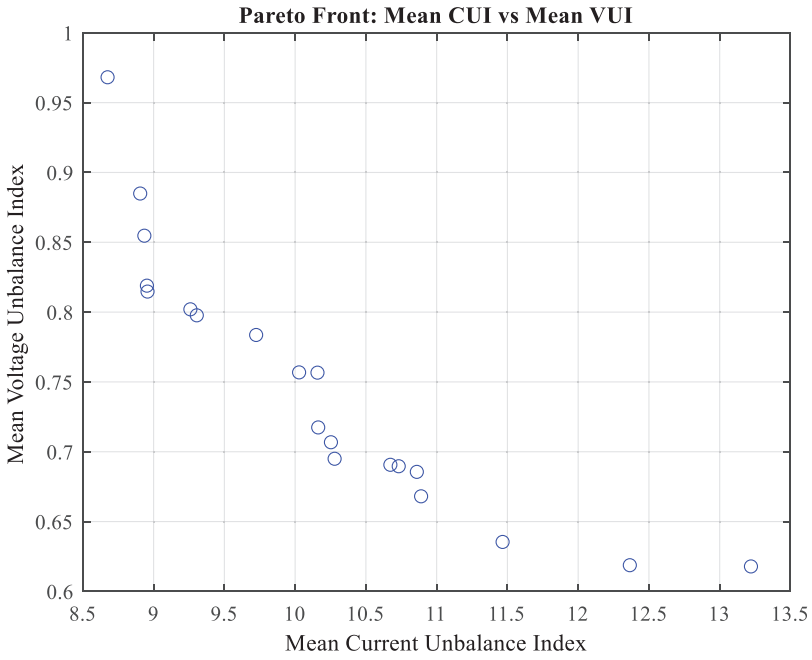

Figure 26: 2-D Pareto front depicting the trade-off between Mean CUI and Mean VUI

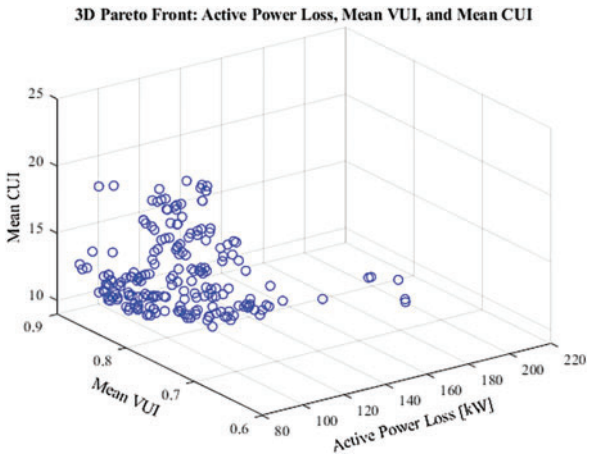

Figure 27: 3-D Pareto surface illustrating the complex relationships among active power loss, mean VUI, and mean CUI

This multi-objective optimization approach represents a significant advancement in power distribution system reconfiguration strategies. By simultaneously addressing power loss, voltage stability, and current balance, the methodology provides a more nuanced and realistic approach to system optimization than traditional single-objective methods. The Pareto-optimal solutions derived from this study offer system operators and planners a spectrum of configuration options, each representing a unique balance of system priorities. This flexibility allows for adaptive decision-making based on specific operational contexts, regulatory requirements, or long-term strategic goals.

6 Conclusion

This study provides a detailed analysis of the reconfiguration problem in unbalanced power distribution networks, focusing on the complex 123-Bus test system. By retaining all components including capacitor banks, voltage regulators, and transformers, the research offers insights more closely aligned with real-world scenarios than previous studies.

The evaluation of twelve metaheuristic algorithms across three distinct scenarios has yielded several significant findings:

- Strategic network reconfiguration can achieve simultaneous optimization of power loss reduction and voltage profile improvement.
- Current and voltage unbalance indices can be effectively minimized under various operational conditions, contributing to improved power quality and system stability.
- The multi-objective optimization approach, utilizing Pareto front analysis, successfully demonstrated the ability to concurrently optimize active current unbalance index, power loss, and voltage unbalance index.

Rigorous statistical analysis identified the AHA as the most efficient algorithm for solving the RecPrb in the 123-Bus UPDN. This finding provides valuable guidance for network operators and researchers in selecting appropriate optimization techniques for UPDN reconfiguration.

The results of this study have important implications for the field of power distribution network management. By addressing the challenges posed by unbalanced loads and considering both current and voltage unbalance, this research contributes to the development of more robust and efficient distribution systems. Future research directions could include:

- Investigating the performance of these algorithms on larger and more complex UPDN systems.
- Incorporating additional objectives such as reliability indices or environmental factors into the optimization problem.
- Exploring the integration of distributed energy resources and their impact on network reconfiguration strategies.
- Developing hybrid algorithms that combine the strengths of multiple metaheuristic approaches for enhanced performance.

In conclusion, this study advances the understanding of UPDN reconfiguration and provides a solid foundation for future research and practical applications in the field of power distribution network optimization and management.

Acknowledgement: The author gratefully acknowledges TÜBİTAK for their valuable support. During the preparation of this work, the author used ChatGPT 4.0-mini in order to refine the English wording of certain phrases. After using this tool/service, the author reviewed and edited the content as needed and takes full responsibility for the content of the publication.

Funding Statement: This work is supported by the Scientific and Technological Research Council of Turkey (TÜBİTAK) under Grant No. 124E002 (1001-Project).

Availability of Data and Materials: The data that support the findings of this study are available from the corresponding author upon reasonable request.

Ethics Approval: Not applicable.

Conflicts of Interest: The author declares no conflicts of interest to report regarding the present study.

Abbreviations

AHA	Artificial Hummingbird Algorithm
AI	Artificial Intelligence
AOA	Arithmetic Optimization Algorithm
ASSA	Artificial Satellite Search Algorithm
BES	Bald Eagle Search
BFS/BFLF	Backward-Forward Sweep Load Flow
CUI	Current Unbalance Index
CVU	Current and Voltage Unbalance
DE	Differential Evolution
DG	Distributed Generation
DRA	Divine Religions Algorithm
Δ-Δ	Delta-Delta transformer connection
Δ-Y	Delta-Wye transformer connection
EO	Equilibrium Optimizer
ENS	Energy Not Supplied (index)
Eq./Eq.'s	Equation/Equations
FDA	Flow Direction Algorithm
FGO	Fungal Growth Optimizer
GBO	Gradient-Based Optimizer
GNDO	Generalized Normal Distribution Optimization
IEEE-PES	Institute of Electrical and Electronics Engineers-Power & Energy Society
INFO	Weighted Mean of Vectors (algorithm)

IoT	Internet of Things
ITSOA	Improved Transient Search Optimization Algorithm
KCL	Kirchhoff's Current Law
MPA	Marine Predator Algorithm
NFL	No Free Lunch (theorem)
PDN	Power Distribution Network
PQ	Power Quality
PQD	Power Quality Disturbance
RE	Relative Error
RecPrb	Reconfiguration Problem
RKO	Runge-Kutta Optimization
SBAT	Selective Bat Algorithm
SMA	Slime Mould Algorithm
SS	Sectionalizing Switch
TLBO	Teaching Learning-Based Optimization
ToV	Table of Visit
TS	Tie Switch/Tie-Switch
UBFS	Unbalanced Backward-Forward Sweep
UPDN	Unbalanced Power Distribution Network
UI	Unbalance Index
UPDN	Unbalanced Power Distribution Network
UPQC	Unified Power Quality Conditioner
VUI	Voltage Unbalance Index
WMs	MATLAB simulation platform developed by the authors
Y-Δ	Wye-Delta transformer connection

Mathematical Symbols and Variables for Section-2

Symbol	Definition
B	Incidence matrix of the network
B'	Modified incidence matrix after removing the reference node
b_{ij}	Elements of the incidence matrix
$I_{i,\phi}$	Current flowing through branch i for phase ϕ
$I_{i,\phi}^{max}$	Maximum allowable current for branch i for phase Φ
N_{Gen}	Number of generators in the system
N_{Load}	Number of loads in the system
N_{Branch}	Number of branches in the system
$P_{i,\phi}^{Gen}$	Generated power at bus i for phase Φ
$P_{i,\phi}^{Load}$	Load power at bus i for phase Φ
$P_{i,\phi}^{Loss}$	Power loss at bus i for phase Φ
$P_{i,Equipment}^{Loss}$	Total equipment losses (transformers, voltage regulators, etc.)
P_L	Total active power loss in the network
$\theta_{i,\phi,cap}^{min}$	Minimum reactive power limit of capacitor bank at bus i for phase ϕ
$\theta_{i,\phi,cap}^{max}$	Maximum reactive power limit of capacitor bank at bus i for phase ϕ
$\theta_{i,\phi,cap}$	Reactive power of capacitor bank at bus i for phase ϕ
$R_{i,\phi}$	Resistance of branch i for phase ϕ
$S_{i,\phi,line}$	Apparent power flow on line i for phase Φ
$S_{i,\phi,line}^{max}$	Maximum permissible apparent power flow on line i for phase ϕ
$Tap_{i,\phi}^{min}$	Minimum tap position of voltage regulator i for phase Φ
$Tap_{i,\phi}^{max}$	Maximum tap position of voltage regulator i for phase Φ

$Tap_{i,\phi}$	Tap position of voltage regulator *i* for phase Φ
$V_{i,\phi}^{min}$	Minimum permissible voltage at bus *i* for phase Φ
$V_{i,\phi}^{max}$	Maximum permissible voltage at bus *i* for phase Φ
$V_{i,\phi}$	Voltage at bus *i* for phase Φ
$V_{i,\phi,Tap}^{min}$	Minimum voltage at the tap position for bus *i* and phase Φ
$V_{i,\phi,Tap}^{max}$	Maximum voltage at the tap position for bus *i* and phase Φ
$V_{i,\phi,Tap}$	Voltage at the tap position for bus *i* and phase Φ
$X_{i,\phi}^{trf_{min}}$	Minimum reactance limit of transformer *i* for phase ϕ
$X_{i,\phi}^{trf_{max}}$	Maximum reactance limit of transformer *i* for phase ϕ
$X_{i,\phi}^{trf}$	Reactance of transformer *i* for phase ϕ
X_{neg}	Negative sequence component
X_{pos}	Positive sequence component

Mathematical Symbols and Variables for Section-3

Symbol	Definition
a	Dimension of the search space
α(alpha)	Guided factor following a normal distribution N(0, 1)
A_i	Direction-switching vector
b	Territorial factor following a normal distribution N(0, 1)
b_{low}	Lower bound of the search space
b_{up}	Upper bound of the search space
D(j)	Permutation function
f	Fitness value associated with the food source
k	Range for random permutation
N(0, 1)	Normal distribution with mean 0 and standard deviation 1
p_i	Position of the i^{th} food source
Rand	Random number in the range [0, 1]
randi (1, a)	Function generating random integers from 1 to a
randperm (k)	Function generating random permutations of integers from 1 to k
r_1	Random number in the range [0, 1]
v_i^{t+1}	Position update value for the i^{th}solution at iteration t + 1
x_i^t	Position of the i^{th} food source at iteration t
$x_{i,target}^t$	Target food source that the i^{th} hummingbird intends to visit at iteration t
x_{worst}^{t+1}	Position of the food source with the lowest nectar replenishment rate at iteration t + 1

Mathematical Symbols and Variables for Section-4

Symbol	Definition
α	Transformer turns ratio (primary voltage/secondary voltage)
D_j	Set of nodes directly connected to node j
ΔT^{abc}	Tap position matrix
ΔV_{max}	Maximum voltage mismatch between consecutive iterations
ε	Convergence criterion (10^{-6} p.u.)
f (·)	Function characterizing voltage dependency according to load type
I_a^p, I_b^p, I_c^p	Currents of phases a, b, c on the primary side of the transformer
I_a^s, I_b^s, I_c^s	Currents of phases a, b, c on the secondary side of the transformer
I_{ij}^{abc}	Three-phase current vector flowing from node i to node j
I_{load}^{abc}	Three-phase load current vector
I_{IEEE}^{abc}	Reference current values from IEEE-123 Bus system documentation
I_{RE}	Current Relative Error
I_{WMs}^{abc}	Three-phase current vector obtained from MATLAB implementation

k_i	Distribution factor (typically 0.5 for uniform distribution)
n_φ	Tap level for phase φ $\left(n_\varphi \in \{-16, -15, \ldots, 0, \ldots, 15, 16\}\right)$
φ	Phase indicator, representing one of the phases $\varphi \in \{a, b, c\}$.
P_{loss} (kW)	Active power losses (kW)
Q_{loss} (kVAr)	Reactive power losses (kVAr)
S_{abc}	Three-phase complex power consumption/load
S_i, S_j	Portions of the load allocated to connection points i and j
S_{load}^{abc}	Three-phase complex power demand/load
S_{loss} (kVA)	Apparent power losses (kVA)
S_0^{abc}	Nominal (reference) three-phase complex power value
S_{total}	Total distributed load value
T_φ	Tap position value for phase φ $\left(T_\varphi = n_\varphi \times 0.00625 \text{ p.u.}\right)$
V_j^{abc}	Three-phase voltage vector at node j
V_{IEEE}^{abc}	Reference voltage values from IEEE-123 Bus system documentation
V_{min} (pu)	Minimum voltage value in the system (p.u.)
V_{max} (pu)	Maximum voltage value in the system (p.u.)
V_p^{abc}	Three-phase voltage vector on the primary side of the transformer
V_{RE}	Voltage Relative Error
V_s^{abc}	Three-phase voltage vector on the secondary side of the transformer
V_{WMs}^{abc}	Three-phase voltage vector obtained from MATLAB implementation
V_0	Nominal voltage value (reference value, 1.0 p.u.)
Y_j^{abc}	Three-phase admittance matrix at node j
Z_{abc}	Phase impedance matrix for three-phase lines
Z_{aa}, Z_{bb}, Z_{cc}	Self-impedances of phases a, b, and c (diagonal elements)
Z_{ab}, Z_{bc}, Z_{ca} etc.	Mutual impedances between phases (off-diagonal elements)
Z_{ij}^{abc}	Three-phase impedance matrix of the branch connecting nodes i and j

References

1. Wang JC, Chiang HD, Darling GR. An efficient algorithm for real-time network reconfiguration in large scale unbalanced distribution systems. IEEE Trans Power Syst. 1996;11(1):511–7. doi:10.1109/59.486141.
2. Lotfi H, Hajiabadi ME, Parsadust H. Power distribution network reconfiguration techniques: a thorough review. Sustainability. 2024;16(23):10307. doi:10.3390/su162310307.
3. Zheng W, Huang W, Hill DJ. A deep learning-based general robust method for network reconfiguration in three-phase unbalanced active distribution networks. Int J Electr Power Energy Syst. 2020;120(2):105982. doi:10.1016/j.ijepes.2020.105982.
4. Cikan M. Multi-objective approaches for optimizing 37-bus power distribution systems with reconfiguration technique: from unbalance current & voltage factor to reliability indices. Comput Model Eng Sci. 2025;143(1):673–721. doi:10.32604/cmes.2025.061699.
5. Cikan M, Cikan NN, Kekezoglu B. Determination of optimal island regions with simultaneous DG allocation and reconfiguration in power distribution networks. IET Renew Power Gener. 2025;19(1):e12942. doi:10.1049/rpg2.12942.
6. Abdel-Basset M, Mohamed R, Abouhawwash M. Fungal growth optimizer: a novel nature-inspired metaheuristic algorithm for stochastic optimization. Comput Methods Appl Mech Eng. 2025;437(10):117825. doi:10.1016/j.cma.2025.117825.
7. Cheng MY, Sholeh MN. Artificial satellite search: a new metaheuristic algorithm for optimizing truss structure design and project scheduling. Appl Math Model. 2025;143(3):116008. doi:10.1016/j.apm.2025.116008.
8. Sultana B, Mustafa MW, Sultana U, Bhatti AR. Review on reliability improvement and power loss reduction in distribution system via network reconfiguration. Renew Sustain Energy Rev. 2016;66(7):297–310. doi:10.1016/j.rser.2016.08.011.

9. Mishra S, Das D, Paul S. A comprehensive review on power distribution network reconfiguration. Energy Syst. 2017;8(2):227–84. doi:10.1007/s12667-016-0195-7.
10. Yang F, Li Z. Effects of balanced and unbalanced distribution system modeling on power flow analysis. In: 2016 IEEE Power & Energy Society Innovative Smart Grid Technologies Conference (ISGT); 2016 Sep 6–9; Minneapolis, MN, USA. doi:10.1109/ISGT.2016.7781195.
11. Cikan M, Kekezoglu B. Comparison of metaheuristic optimization techniques including equilibrium optimizer algorithm in power distribution network reconfiguration. Alex Eng J. 2022;61(2):991–1031. doi:10.1016/j.aej.2021.06.079.
12. Parihar SS, Malik N. Network reconfiguration in the presence of optimally integrated multiple distributed generation units in a radial distribution network. Eng Optim. 2024;56(5):679–99. doi:10.1080/0305215x.2023.2187790.
13. Abbas G, Wu Z, Ali A. Multi-objective multi-period optimal site and size of distributed generation along with network reconfiguration. IET Renew Power Gener. 2024;18(16):3704–30. doi:10.1049/rpg2.12949.
14. Li JY, Chen JJ, Wang YX, Chen WG. Combining multi-step reconfiguration with many-objective reduction as iterative bi-level scheduling for stochastic distribution network. Energy. 2024;290:130198. doi:10.1016/j.energy.2023.130198.
15. Naderipour A, Abdullah A, Marzbali MH, Arabi Nowdeh S. An improved corona-virus herd immunity optimizer algorithm for network reconfiguration based on fuzzy multi-criteria approach. Expert Syst Appl. 2022;187(8):115914. doi:10.1016/j.eswa.2021.115914.
16. Zhai HF, Yang M, Chen B, Kang N. Dynamic reconfiguration of three-phase unbalanced distribution net-works. Int J Electr Power Energy Syst. 2018;99:1–10.
17. Kaur M, Ghosh S. Network reconfiguration of unbalanced distribution networks using fuzzy-firefly algorithm. Appl Soft Comput. 2016;49(2):868–86. doi:10.1016/j.asoc.2016.09.019.
18. Jacob RA, Paul S, Li W, Chowdhury S, Gel YR, Zhang J. Reconfiguring unbalanced distribution networks using reinforcement learning over graphs. In: 2022 IEEE Texas Power and Energy Conference (TPEC); 2022 Feb 28–Mar 1; College Station, TX, USA. doi:10.1109/TPEC54980.2022.9750805.
19. Gangwar P, Singh SN, Chakrabarti S. Network reconfiguration for unbalanced distribution systems. In: TENCON 2017–2017 IEEE Region 10 Conference; 2017 Nov 5–8; Penang, Malaysia. p. 3028–32. doi:10.1109/TENCON.2017.8228381.
20. Duran-Quintero M, Candelo JE, Soto-Ortiz J. A modified backward/forward sweep-based method for reconfiguration of unbalanced distribution networks. Int J Electr Comput Eng. 2019;9(1):85. doi:10.11591/ijece.v9i1.pp85-101.
21. Gerez C, Costa ECM, Sguarezi Filho AJ. Static reconfiguration of unbalanced distribution systems with variable power using selective bat algorithm. J Control Autom Electr Syst. 2021;32(3):656–71. doi:10.1007/s40313-021-00695-z.
22. Zhou A, Zhai H, Yang M, Lin Y. Three-phase unbalanced distribution network dynamic reconfiguration: a distributionally robust approach. IEEE Trans Smart Grid. 2022;13(3):2063–74. doi:10.1109/TSG.2021.3139763.
23. Amanulla B, Chakrabarti S, Singh SN. Reconfiguration of power distribution systems considering reliability and power loss. IEEE Trans Power Deliv. 2012;27(2):918–26. doi:10.1109/TPWRD.2011.2179950.
24. Mehroliya S, Arya A. Distributed generator and capacitor-embedded reconfiguration in three-phase unbalanced distribution systems using teaching learning-based optimization. Comput Appl Eng Educ. 2024;32(1):e22689. doi:10.1002/cae.22689.
25. Caicedo JE, Agudelo-Martínez D, Rivas-Trujillo E, Meyer J. A systematic review of real-time detection and classification of power quality disturbances. Prot Control Mod Power Syst. 2023;8(1):3. doi:10.1186/s41601-023-00277-y.
26. Bollen MHJ. What is power quality? Electr Power Syst Res. 2003;66(1):5–14.
27. Alanazi M, Alanazi A, Almadhor A, Memon ZA. Multiobjective reconfiguration of unbalanced distribution networks using improved transient search optimization algorithm considering power quality and reliability metrics. Sci Rep. 2022;12(1):13686. doi:10.1038/s41598-022-17881-x.

28. Arghavani H, Peyravi M. Unbalanced current-based tariff. CIRED Open Access Proc J. 2017;2017(1):883–7. doi:10.1049/oap-cired.2017.0129.
29. Beneteli TAP, Cota LP, Euzébio TAM. Limiting current and voltage unbalances in distribution systems: a metaheuristic-based decision support system. Int J Electr Power Energy Syst. 2022;135:107538. doi:10.1016/j.ijepes.2021.107538.
30. Pillay P, Manyage M. Definitions of voltage unbalance. IEEE Power Eng Rev. 2001;21(5):49–51. doi:10.1109/MPER.2001.4311362.
31. Cikan M, Cikan NN. Optimum allocation of multiple type and number of DG units based on IEEE 123-bus unbalanced multi-phase power distribution system. Int J Electr Power Energy Syst. 2023;144(10):108564. doi:10.1016/j.ijepes.2022.108564.
32. Gerez C, Coelho Marques Costa E, Sguarezi Filho AJ. Distribution network reconfiguration considering voltage and current unbalance indexes and variable demand solved through a selective bio-inspired metaheuristic. Energies. 2022;15(5):1686. doi:10.3390/en15051686.
33. Nacar Cikan N, Cikan M. Reconfiguration of 123-bus unbalanced power distribution network analysis by considering minimization of current & voltage unbalanced indexes and power loss. Int J Electr Power Energy Syst. 2024;157:109796.
34. Li S, Chen H, Wang M, Heidari AA, Mirjalili S. Slime mould algorithm: a new method for stochastic optimization. Future Gener Comput Syst. 2020;111:300–23. doi:10.1016/j.future.2020.03.055.
35. Faramarzi A, Heidarinejad M, Stephens B, Mirjalili S. Equilibrium optimizer: a novel optimization algorithm. Knowl Based Syst. 2020;191:105190. doi:10.1016/j.knosys.2019.105190.
36. Storn R, Price K. Differential evolution—a simple and efficient heuristic for global optimization over continuous spaces. J Glob Optim. 1997;11(4):341–59.
37. Zhao W, Wang L, Mirjalili S. Artificial hummingbird algorithm: a new bio-inspired optimizer with its engineering applications. Comput Methods Appl Mech Eng. 2022;388(1):114194. doi:10.1016/j.cma.2021.114194.
38. Dey I, Roy PK. Simultaneous network reconfiguration and DG allocation in radial distribution networks using arithmetic optimization algorithm. Int J Numerical Modelling. 2023;36(6):e3105. doi:10.1002/jnm.3105.
39. Alsattar HA, Zaidan AA, Zaidan BB. Novel meta-heuristic bald eagle search optimisation algorithm. Artif Intell Rev. 2020;53(3):2237–64. doi:10.1007/s10462-019-09732-5.
40. Karami H, Anaraki MV, Farzin S, Mirjalili S. Flow direction algorithm (FDA): a novel optimization approach for solving optimization problems. Comput Ind Eng. 2021;156(4):107224. doi:10.1016/j.cie.2021.107224.
41. Ahmadianfar I, Bozorg-Haddad O, Chu X. Gradient-based optimizer: a new metaheuristic optimization algorithm. Inf Sci. 2020;540:131–59. doi:10.1016/j.ins.2020.06.037.
42. Zhang Y, Jin Z, Mirjalili S. Generalized normal distribution optimization and its applications in parameter extraction of photovoltaic models. Energy Convers Manag. 2020;224(9):113301. doi:10.1016/j.enconman.2020.113301.
43. Ahmadianfar I, Heidari AA, Noshadian S, Chen H, Gandomi AH. INFO: an efficient optimization algorithm based on weighted mean of vectors. Expert Syst Appl. 2022;195(12):116516. doi:10.1016/j.eswa.2022.116516.
44. Faramarzi A, Heidarinejad M, Mirjalili S, Gandomi AH. Marine predators algorithm: a nature-inspired metaheuristic. Expert Syst Appl. 2020;152(4):113377. doi:10.1016/j.eswa.2020.113377.
45. Ebeed M, Mostafa A, Aly MM, Jurado F, Kamel S. Stochastic optimal power flow analysis of power systems with wind/PV/TCSC using a developed Runge Kutta optimizer. Int J Electr Power Energy Syst. 2023;152(20):109250. doi:10.1016/j.ijepes.2023.109250.
46. Ma K, Fang L, Kong W. Review of distribution network phase unbalance: scale, causes, consequences, solutions, and future research directions. CSEE J Power Energy Syst. 2020;6(3):479–88. doi:10.36227/techrxiv.11401056.v2.
47. Tiwari S, Agrawal R, Agrawal D, Verma D. Performance analysis of DVR and UPQC to improve power quality of three-phase distribution system. In: 2021 IEEE 2nd International Conference on Electrical Power and Energy Systems (ICEPES); 2021 Dec 10–11; Bhopal, India. doi:10.1109/ICEPES52894.2021.9699503.
48. IEEE PES distribution systems analysis subcommittee radial test feeders [Internet]. [cited 2024 Sep 17]. Available from: https://cmte.ieee.org/pes-testfeeders/resources/.